Hindawi
Advances in Meteorology
Volume 2023, Article ID 3956086, 23 pages
https://doi.org/10.1155/2023/3956086

Research Article

Modes of Atmospheric Energetics Based on HadGEM3-GC3.1-LL Simulations in the Framework of CMIP6

Silas Michaelides

Climate and Atmosphere Research Centre (CARE-C), The Cyprus Institute, Nicosia, Cyprus

Correspondence should be addressed to Silas Michaelides; silas.michaelides@gmail.com

Received 10 May 2023; Revised 31 July 2023; Accepted 7 August 2023; Published 2 September 2023

Academic Editor: Pedro Salvador

In this study, the focus is on investigating how different climate scenarios, as they have been adopted in Phase 6 of the Coupled Model Intercomparison Project (CMIP6), can lead to different regimes in the energetics components in Lorenz's energy cycle, hence impacting the "working rate" of the climate system, which is considered as a "heat engine." The four energy forms on which this investigation is based on are the zonal and eddy components of the available potential and kinetic energies. The permissible correspondingly considered transformations between these forms of energy are also studied. Generation of available potential energy and dissipation of kinetic energy complete the Lorenz energy cycle that is adopted here. In the CMIP6 approach, the results of different climate change analyses were collected in a matrix defined by two dimensions: climate exposure as characterized by a radiative forcing or temperature level and socioeconomic development as classified by the pathways, known as Shared Socioeconomic Pathways (SSPs). The basis of the calculations in this study is the climatic projection produced by the HadGEM3-GC3.1-LL climatic model in the period from 2015 to 2100. In this respect, the results are presented in terms of time projections of the energetics components under different SSPs. The results have shown that the different SSPs yield diverse energetics regimes, consequently impacting on Lorenz energy cycle and, hence, a "working rate" of the climate system based on the components of this cycle. In this respect, Lorenz energy cycle projections are presented, under different SSPs. The results are also contrasted to the calculations for the historical period 1929 to 2014 as this is simulated by the same climatic model.

1. Introduction

The study of the fate of atmospheric energy can form a basis for contemplating the climate system as a heat engine. Within this conceptual framework, atmospheric thermodynamic energy is converted into atmospheric kinetic energy with the latter ultimately dissipated into heat. Since the large-scale atmospheric processes have long been recognized to be governed by eddy motions (see[1]), the study of the fate of atmospheric energy, as this is determined by Lorenz's energy cycle [2–4], appears to comprise a rational basis for scientific investigations on the efficiency with which energy atmospheric energy is generated, converted, and dissipated under different climate change scenarios. Indeed, the overall strength of Lorenz's energy cycle yields a "rate of working" of the climate [5].

Improving our knowledge of climate change lies in the focus of the Coupled Model Intercomparison Project (CMIP) of the World Climate Research Programme (WCRP). CMIP is a unique international collaborative framework fostering a systematic assessment of climate change impacts on the basis of model outputs from a large number of General Circulation Models (GCM). This scientific endeavor has gone through various phases, the most recent of which being CMIP Phase 6 (CMIP6). Details of the experimental design and the organisation of CMIP6 are provided in an overview paper by Eyring et al. [6]. Output data fields from CMIP6 are becoming available to the community for analysis and exploitation, addressing a wide range of specific questions and filling scientific gaps of previous CMIP phases [6], in time for inclusion in the Sixth Assessment Report (AR6) of the Intergovernmental Panel on Climate Change (IPCC). An integral part of CMIP6 is the definition of the experimental design and eventual documentation of the simulations which provide a comprehensive description of how the experiments are executed [7].

In the present study, output from the Scenario Model Intercomparison Project (ScenarioMIP) has been used. ScenarioMIP comprises a primary activity within the context of CMIP6, providing multimodel climate projections based on alternative climate scenarios that are pertinent to societal concerns regarding climate change mitigation, adaptation, or impacts [7]. The climate projections adopted in ScenarioMIP are driven by a new set of Shared Socioeconomic Pathways (SSPs) produced with integrated assessment models based on new future pathways of societal development but also incorporating the previously used Representative Concentration Pathways (RCPs) [8]. The scenario matrix architecture that underlies the framework for formulating new scenarios for climate research is described by van Vuuren et al. [9]; this scenario matrix is based on two main axes: one representing the level of radiative forcing of the climate system (characterized by the RCPs), and the other representing a set of alternative plausible trajectories of future global development (characterized by the SSPs).

RCPs comprise future climate scenarios which were adopted in CMIP6's predecessor, namely, CMIP5 (the Coupled Model Intercomparison Project Phase 5 [10]); within the framework of the CMIP5 project, a number of future scenarios of radiative forcing due to greenhouse emissions had been established, yielding four Representative Concentration Pathways (RCPs): one high pathway for which radiative forcing reaches >8.5 Wm^{-2} by year 2100 and continues to rise for some amount of time (termed as RCP8.5); two intermediate "stabilization pathways" in which radiative forcing is stabilized at approximately 6 Wm^{-2} and 4.5 Wm^{-2} after year 2100 (RCP6.0 and RCP4.5, respectively); and one pathway where radiative forcing peaks at approximately 2.6 Wm^{-2} before year 2100, declining afterwards (RCP2.6).

The need for new pathways for use in future climate change studies was recognized even during the execution of CMIP5 and before the current CMIP6 started. Key challenges for using socioeconomic scenarios for climate change analyses were early advocated by several research groups [11, 12], in an effort to amplify the setting up of climate scenarios for CMIP6. A family of SSP scenarios embracing a variety of possible future socioeconomic features has been under discussion for some time [13, 14], with five SSPs being eventually determined, namely, SSP1, SSP2, SSP3, SSP4, and SSP5. For a comprehensive illustration of these five SSPs, O'Neill et al. [15] juxtaposed them onto a conceptual two-axis framework; each axis was constructed on the basis of a group of socioeconomic challenges: one axis is based on challenges to mitigation and the other on challenges to adaptation. By dividing this "challenge space" in five domains, each of the five SSPs can subsequently be mapped onto this conceptual two-dimensional space, such that each of the five domains represents each of the SSPs: SSP1 embraces the low challenges, while SSP3 embraces high challenges; SSP4 is deployed in the domain where adaptation challenges dominate, while SSP5 represents the area where mitigation challenges dominate. In the centre of the "challenge space" lies an intermediate challenge pathway, namely, SSP2.

The RCP-SSP matrix architecture adopted in ScenarioMIP yields future scenarios which combine different socioeconomic reference assumptions (as described by SSPs) with different future levels of climate forcing (as described by RCPs) [9]. Of the total number of the available scenarios, a subset has been selected for inclusion in ScenarioMIP simulations [16]. The following three scenarios under Tier 1 of ScenarioMIP are used in the present study:

(i) ssp126: An SSP-based concentration-driven scenario with low radiative forcing by the end of the century. Following approximately the RCP2.6 global forcing pathway with SSP1 socioeconomic conditions, radiative forcing reaches a level of 2.6 W/m^2 in 2100.

(ii) ssp245: An SSP-based concentration-driven scenario with medium radiative forcing by the end of the century. Following approximately the RCP4.5 global forcing pathway with SSP2 socioeconomic conditions, radiative forcing reaches a level of 4.5 W/m^2 in 2100.

(iii) ssp585: An SSP-based concentration-driven scenario with high radiative forcing by the end of century. Following approximately the RCP8.5 global forcing pathway with SSP5 socioeconomic conditions, radiative forcing reaches a level of 8.5 W/m^2.

(iv) In addition to the above three future scenarios, the historical data within the same cohort have been used for comparative purposes. The historical data used herein cover the period from 1929 to 2014.

The objective of this study is to examine how different SSPs impact the fate of atmospheric energy within the framework of Lorenz energy cycle. The investigation is further extended with a comparative study of the "rate of working" of the climate system in terms of the efficiency of energy generation, conversion, and dissipation.

Following this introduction, Section 2 briefly reviews the fundamentals of the Lorenz energy cycle and the literature on its exploitation in climate change studies. Section 3 describes the data that have been used, including also a brief outline of the climatic model used. Section 4 describes the numerical methodology adopted. The results are presented in Section 5: Section 5.1 presents the energy balance and Section 5.2 presents the time series and trends of the energetics components under different SSP-based scenarios. Section 5.3 presents the results on the extremes of the energy components and Section 5.4 is devoted to a brief discussion of the efficiency of energy conversion of the atmospheric heat engine. Section 6 comprises the discussion part that includes some future plans.

2. Fate of Atmospheric Energy: Lorenz Energy Cycle

With regard to the various forms of energy that are present in the atmosphere, kinetic energy has received the most attention. Often, the kinetic energy of a weather system is regarded as a measure of its intensity. The only other forms

of atmospheric energy which appear to play a major role in the energy budget of the troposphere and lower stratosphere are the potential energy, the internal energy, and the latent energy of water vapor. Potential and internal energy may be transformed directly into kinetic energy, while latent energy may be transformed directly into internal energy, which is then transformed into kinetic energy.

It is easily shown by means of the hydrostatic approximation that the changes of the potential energy and the internal energy of the whole atmosphere are approximately proportional, so that it is convenient to regard potential and internal energy as constituting a single form of energy. This form has been called total potential energy by Margules [17]. Expanding Margules' [17] approach in considering a hypothetical adiabatic redistribution of the mass of the atmosphere, Lorenz [2, 4] introduced the concept ofavailable potential energy as the part of potential and internal energies (collectively termed as total potential energy), which is available for conversion into kinetic energy. The amount of total potential energy that is not converted into kinetic energy comprises a reference state of minimum energy reached through an adiabatic redistribution of the mass of the atmosphere.

Lorenz [2, 3] has shown that a partial explanation of the intensity of the energy cycle can be obtained by considering the concept of available potential energy. Available potential energy does not represent a supply of energy additional to the forms already mentioned, but instead represents a portion of the total potential energy which may be available for conversion into kinetic energy. The available potential energy of the atmosphere has been defined by Lorenz [2, 3] as the difference between the total potential energy held by the atmosphere at a given state and the minimum total potential energy which could result from any adiabatic redistribution of the mass of the atmosphere. Available potential energy can be generated principally by either heating of the warmer regions and cooling of the colder regions at the same elevation, on the one hand, and by heating of the lower and cooling of the higher levels (leading to a decrease of static stability), on the other hand. Through a reversible adiabatic process, available potential energy is converted into kinetic energy, whereas the latter is dissipated by friction. The deliberations briefly discussed in this paragraph determine a basic three-step energy "cycle": available potential energy is generated through diabatic processes and may subsequently be converted into kinetic energy which is in turn dissipated by friction.

The discussion of the energy forms and their transformations does not relate to individual or particular weather systems. The application of these concepts to a limited area of the atmosphere (e.g., the stratosphere, see [18, 19]) or surrounding discrete weather systems (e.g., [20]) presents both conceptual and computational uncertainties which should be borne in mind.

With the increase of atmospheric measurements pertaining to the large-scale systems, the interest in atmospheric energetics has become more intense in the second half of the twentieth century with several published investigations on kinetic energy (e.g., [21]). However, Lorenz's framework for the fate of atmospheric energy, as discussed below, has further enhanced the interest of the scientific community in atmospheric energetics because it provides a broader basis on which the dynamics of the atmosphere can be studied in more detail. Lorenz's framework has revitalized the interest in the atmospheric energetics (e.g., [22–25]).

The concept of available potential energy has been widely incorporated in studies of general circulation and large-scale dynamics [26]. Following its original introduction by Lorenz, alternative propositions and reformulations have been proposed, employing further refinements (e.g., [22, 25, 27]). The concept available potential energy is still under scrutiny from different viewpoints (e.g., [28, 29]).

Lorenz has postulated a basic flow of energy comprising of diabatic generation which adds to the pool of available potential energy; adiabatic conversion of available potential energy adds to the pool of kinetic energy which is subsequently dissipated by frictional processes.

Bearing in mind that the atmospheric motions can be decomposed into zonal and eddy parts, available potential and kinetic energies were further partitioned into zonal and eddy components; this conceptualization refines the above energy flow into an energy cycle involving zonal and eddy energy generation and dissipation, as well as four physically founded energy conversions, as they are detailed in Figure 1. The quantities in the four circles indicate the four pools of energy: zonal available potential energy (AZ), eddy available potential energy (AE), zonal kinetic energy (KZ), and eddy kinetic energy (KE) (for a list of symbols used herein, see Appendix A).

Regarding the energy conversion terms in the cycle, the direction of the mean energy flow, as conceptualized by Lorenz, is retained, so that the arrows in the figure indicate positive values.

On the one hand, the generation of AZ, which is denoted by GZ, is accomplished through a process described by diabatic heating of the lower latitude zones and diabatic cooling of the higher latitude zones; on the other hand, diabatic heating of warmer regions and cooling of colder ones at the same latitude lead to the generation of AE that is denoted by GE. Both of these generation terms of zonal and eddy available potential energies are considered as positive inputs to the respective available potential energy reservoirs.

The dissipation of zonal and eddy kinetic energies, denoted by DZ and DE, respectively, is considered as negative inputs (or sinks) to the respective kinetic energy reservoirs, or equivalently they contribute to diminishing the respective kinetic energy contents; DZ is accomplished by the zonally averaged frictional processes, whereas DE is accomplished by the deviation of the frictional processes from their zonal average.

The process that converts available potential energy into kinetic energy is described as a sinking of colder air and rising of warmer air. This is resolved into two processes. The first is described as accomplished by sinking of colder air in colder latitude zones and rising of warmer air

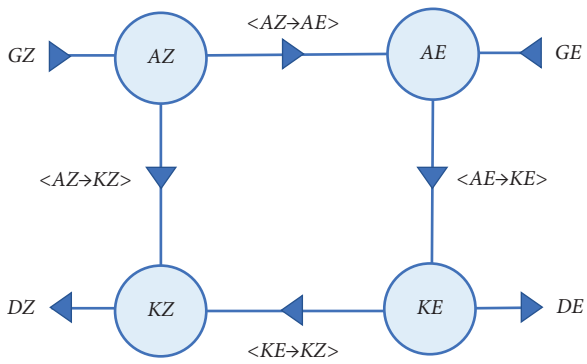

Figure 1: Lorenz energy cycle: circles denote pools of zonal and eddy available potential energies (*AZ* and *AE*, respectively) and pools of zonal and eddy kinetic energies (*KZ* and *KE*, respectively); conversions from one energy form into another are denoted by $<AZ \longrightarrow AE>$, $<AE \longrightarrow KE>$, $<KE \longrightarrow KZ>$, and $<AZ \longrightarrow KZ>$; generation of *AZ* and *AE* is denoted by *GZ* and *GE*, respectively; dissipation of zonal and eddy kinetic energies is denoted by *DZ* and *DE*, respectively.

in warmer latitude zones, denoted by $<AZ \longrightarrow KZ>$. The second is described as sinking of colder air and rising of warmer air within the latitude zone, denoted by $<AE \longrightarrow KE>$.

The process that consists of a horizontal or vertical transport by the eddy motions of angular momentum towards zones of lower average angular velocity converts *KZ* into *KE*; this process tends to equalize the angular velocities of the different zones, thereby reducing the overall kinetic energy of the zonal flow, since among all velocity fields with the same total angular momentum, the field of constant angular velocity has the least kinetic energy; the only sink of *KZ* is the kinetic energy of the eddies themselves, i.e., *KE*. However, observational investigations have long shown that the transport of angular momentum by eddies is predominantly towards zones of higher angular velocity (e.g., westerly jet streams), so that *KE* is converted into *KZ* by the eddies themselves. This is denoted by the conversion term $<KE \longrightarrow KZ>$.

A process that can convert *AZ* into *AE* (without altering the total available potential energy) is a horizontal or vertical transport by the eddies of sensible heat towards zones where temperature is low, relative to the horizontally averaged temperature. This is denoted by $<AZ \longrightarrow AE>$.

3. Materials

3.1. Data. In the present study, use has been made of the climatic projections in the period from 2015 to 2100 (i.e., 86 years), produced by the HadGEM3-GC3.1 model at the LL resolution, denoted by HadGEM3-GC31-LL [30] within the framework of the CMIP6 ScenarioMIP Activity. As explained below, for comparative purposes, the "historical" data from the same model have also been used. The climatic projections and the historical data which were retrieved for the needs of the present study are archived and provided by the *Earth System Grid Federation* (ESGF) [31]. Each year in the dataset is considered to comprise 360 days. With the frequency of the retrieved dataset at one per day, the values of the variables selected are assigned to 1200 UTC; hence, a total of 30960 times are included in the climatic projections and the historical datasets that were used as a basis for this investigation. The data used in the present atmospheric energetics analysis refer to the variant r1i1p1f3 of the model output, where the numbers are indices for particular configurations of *r* (realization, i.e., ensemble member), *i* (initialisation method), *p* (physics), and *f* (forcing). The projections used were retrieved at the model's native grid for the fields of temperature (in K), eastward and northward wind velocity components (in $m \cdot s^{-1}$), and Lagrangian pressure tendency (in $Pa \cdot s^{-1}$), available at a $1.25^{\circ} \times 1.875^{\circ}$ (lat-lon) spatial resolution and at 19 pressure levels, namely, 1000, 925, 850, 700, 600, 500, 400, 300, 250, 200, 150, 100, 70, 50, 30, 20, 10, 5, and 1 hPa. It is useful to clarify at this point that the data used and the results subsequently obtained refer to the global atmosphere and cannot be interpreted within any subregion or in relation to any individual atmospheric motion.

The calculations for the energetics have been carried out using the data for the three of the Tier 1 ScenarioMIP scenarios, namely, the ssp126, ssp245, and ssp585 [32–34]. The corresponding set of the historical data was also used in the calculations for comparative purposes [35]. This dataset has the same specifications as the datasets retrieved for the above three scenarios as explained above but refers to a time period from 1850 till 1914. In the present study, the period of the historical data is taken to have the same 85-year time span as the climatic projections, namely, from 1929 to 2014.

3.2. Model Outline. HadGEM3-GC3.1 is the third Hadley Centre Global Environmental Model. Running in the Global Coupled configuration 3.1 of the Unified Model, it represents the latest climate model of the U.K. Met Office [36]; this is a coupled Earth System Model that was used in the CMIP6 centennial simulations. HadGEM3-GC3.1 incorporates a global atmosphere-land configuration, a global ocean component, sea ice model configuration, and a new modal aerosol scheme. It is beyond the scope of this paper to elaborate on the HadGEM3-GC3.1 model configuration; details on the configuration of the HadGEM3-GC3.1 model are given by Kuhlbrodt et al. [37], Menary et al. [36], and Williams et al. [38].

4. Numerical Methodology

The calculations of the energetics components and their corresponding dynamical processes as they are implicated in the numerical solution of the mathematical expressions describing the cycle's components present by themselves great computational challenges (see [39, 40]). These calculations call for the estimation of horizontal and vertical derivatives, as well as zonal and area averaging and vertical integrations. Limitations imposed on the vertical derivatives and integrals by the lower and upper atmospheric boundaries, as well as on the derivatives and area averages imposed by the singularities at the poles, are few of such challenges requiring special computational handling. The numerical

analogues for the mathematical computations are given in Appendix B.

Bearing in mind that the wind field may be resolved into a zonal component (associated with the zonal flow) and an eddy component (associated with the superimposed eddy motion), the kinetic energy can be resolved into zonal and eddy parts, denoted by KZ and KE, respectively. On analogous arguments, the available potential energy is also partitioned into zonal and eddy components, denoted by AZ and AE, respectively.

In this research, the respective mathematical relationships describing each of the energy forms, conversions, generation, and dissipation terms are those developed by Muench [18, 19] for the zonal and eddy motions in the atmosphere; they are all presented in Appendix C, adopting the notation proposed by Reiter [41], with minor changes by Michaelides [20]. The available potential energy generation (GZ and GE) and dissipation of kinetic energy (DZ and DE) are calculated as residuals to the respective energy balance differential equations, as shown in Appendix D.

5. Results

The energy balance and time series of the energetics components under different SSP-based scenarios show that different scenarios yield diverse energetics regimes, consequently impacting the Lorenz energy cycle and its underlying physical processes.

5.1. Energy Balance. The energy balance for each of the three SSP-based scenarios and for the historical dataset is presented in Figure 2. The values given are averages taken over the entire period 2015–2100 for the SSP-based simulations and for 1929 to 2014 for the historical data.

The AZ reservoir decreases with increasing SSP forcing: from $4783.51 \times 10^3\,\mathrm{Jm}^{-2}$ under ssp126, it drops to $4723.34 \times 10^3\,\mathrm{Jm}^{-2}$ under ssp585. Compared to the reservoir of AZ in the historical data, the AZ reservoir in all three SSP-based scenarios appears to hold less energy than in the historical period.

The AE reservoir behaves the same way as AZ: from $536.94 \times 10^3\,\mathrm{Jm}^{-2}$ under ssp126, it decreases to $526.23 \times 10^3\,\mathrm{Jm}^{-2}$ under the extreme ssp585 one. Also, the AE held in the respective reservoir is less under the future simulations compared to the historical data.

The KZ reservoir is enhanced with increasing SSP forcing: from $962.87 \times 10^{-3}\,\mathrm{Wm}^{-2}$ at ssp126, it increases to $974.43 \times 10^{-3}\mathrm{Wm}^{-2}$ at ssp245 and to $1009.85 \times 10^{-3}\mathrm{Wm}^{-2}$ at ssp585. Clearly, in all the future states, the reservoirs of KZ are larger than the historical one. However, the behavior of KE with increasing SSP forcing is different: from $688.58 \times 10^{-3}\,\mathrm{Wm}^{-2}$ at ssp126, it decreases to $684.15 \times 10^{-3}\,\mathrm{Wm}^{-2}$ at 245 and decreases further to $682.1 \times 10^{-3}\,\mathrm{Wm}^{-2}$ at ssp585, with all the simulated future scenarios yielding less eddy kinetic energy compared to the historical period.

As a general conclusion, it can be said that, overall, it appears that energy is converted more intensely in the historical records rather than in the SSP-based simulations. Both the energy conversions, $<AZ \longrightarrow AE>$ and $<AE \longrightarrow KE>$, decrease in intensity with increasing forcing. Also, compared to the historical period, they both convert energy at lower rates. The $<KE \longrightarrow KZ>$ conversion is also slightly higher in the historical period compared to all the SSP-based scenarios. Lastly, the calculated conversion $<AZ \longrightarrow KZ>$ is higher with the historical data compared to almost all corresponding values with the SSP simulations.

The $<AZ \longrightarrow KZ>$ conversion is by far the smallest of all the conversion terms. Bearing in mind that the conversion between AZ and KZ is accomplished through meridional circulations which are responsible for the large-scale rising and sinking of air, it is worth contemplating at this point the crucial role that the Hadley and Ferrel cells play in this energy conversion process [42–44].

The thermally direct Hadley cell is characterized by rising of warm, light air in equatorial latitudes and sinking of colder, denser air in the subtropical latitudes. This circulation is responsible for a positive conversion, i.e., a conversion from zonal available potential energy into zonal kinetic energy. On the contrary, the thermally indirect Ferrel cell which extends between 30° and 60° latitude circles is characterized by sinking of relatively warm, light air in the subtropical belt and rising of colder, denser air at higher latitudes, yielding a negative conversion, i.e., from zonal kinetic energy to zonal available potential energy.

The two-way $<AZ \longrightarrow KZ>$ conversions in the Hadley and Ferrell cells are nearly equal and opposite (see [45]); therefore, as a global mean, this term is small, as noted above. In particular, comparing $<AZ \longrightarrow KZ>$ to $<KE \longrightarrow KZ>$, it is seen that the latter is approximately five times greater than the former; this finding confirms the importance of the eddying motions in maintaining the zonal kinetic energy reservoir. Indeed, the fate of atmospheric energy is subject to two main processes: baroclinic growth of eddies (connected to heat fluxes) and barotropic decay (connected to momentum fluxes) (see [46–48]). The process of baroclinic growth occurs mainly due to the growth of mid-latitude baroclinic synoptic-scale disturbances, which includes the transformation of the zonal available potential energy into eddy available potential energy through horizontal and vertical transport of sensible heat and the transformation of eddy available potential energy into eddy kinetic energy by rising warm air and sinking cold air.

In the process of barotropic decay, a large part of eddy kinetic energy is dissipated by frictional dissipation (DE) and the remainder is converted back into zonal kinetic energy through horizontal and vertical transport of angular momentum by the eddies (namely, $<KE \longrightarrow KZ>$). Through this latter conversion between the two kinetic energy forms,

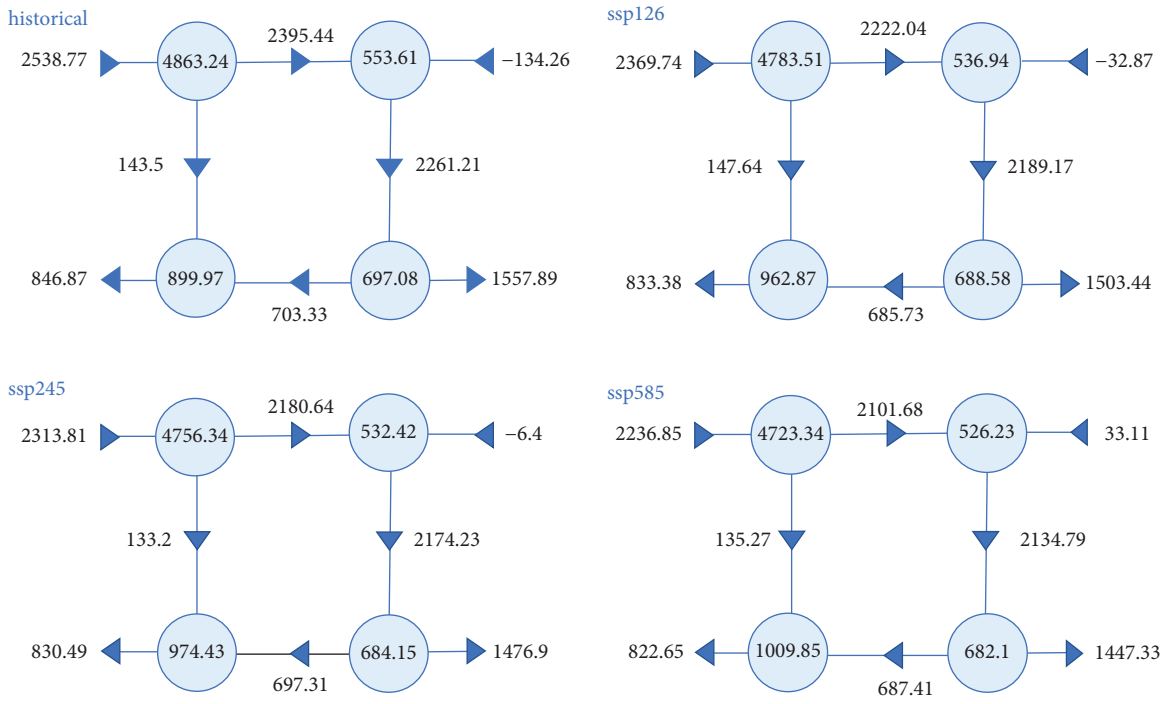

FIGURE 2: Energy budget for different SSP-based scenarios. Energy reservoirs (in circles) are in 10^3 Jm^{-2}; energy conversion, generation, and dissipation are in 10^{-3} Wm^{-2}.

the barotropic decay process ensures the maintenance of the extratropical jet streams and storm tracks [45, 47, 48]. However, with regard to the subtropical jet streams, the barotropic decay does not constitute a primary process for their maintenance, with the conservation of the angular momentum having the major role.

The *GZ* decreases with increasing SSP forcing with all the simulated future scenarios yielding less zonal available potential energy generation than in the historical records. The *GE* appears to act in the direction of depleting the *AE* reservoir under the ssp126 and ssp245 scenarios, but in ssp585, it reverses its sign, thus contributing to enhancing the *AE*. The depletion of *AE* through diabatic processes is more pronounced in the historical data.

Both kinetic energy dissipation terms, *DZ* and *DE*, decrease as the SSP forcing increases. Both terms are less than the corresponding terms calculated with the historical data used. As stated above, during the barotropic decay, eddy kinetic energy is either frictionally dissipated or transformed into zonal kinetic energy. Comparing *DE* and $<AZ \longrightarrow KZ>$ in the present findings, the former has been calculated as approximately twice as much as the latter.

For all SSP-based scenarios but also for the historical records used herein, the sign of the dissipation terms, *DZ* and *DE*, is in agreement with what is expected from the effect of frictional processes, i.e., to dissipate kinetic energy. The transformation of kinetic energy into thermal energy through dissipation is not accounted for in Lorenz energy cycle, as it is adopted here; notwithstanding this presumption in the original contemplation of the energy cycle, Bannon [29] has shown that the feeding back of the frictionally induced thermal energy into the energy cycle is conceivable too.

It is useful at this point to conclude this section by acknowledging an important attribute inherent in the data used in this study, which comprise essentially the output from a model which emulates the future climate of the Earth. In effect, an appreciation of the sensitivity of the model to changes in carbon dioxide concentrations which determine the forcing to the model in use is briefly presented. The determination of the sensitivity of the Earth's climate to changes in atmospheric carbon dioxide is a fundamental goal of climate science [49]. In this respect, the equilibrium climate sensitivity metric is often considered as representing the equilibrium global surface warming in response to a doubling of atmospheric carbon dioxide concentration relative to preindustrial levels [50]. Due to complications arising from a strict approach in calculating the equilibrium climate sensitivity, Gregory et al. [51] have proposed a shortcut for estimating it, known as the Effective Climate Sensitivity, which is widely adopted in CMIP6. Effective Climate Sensitivity is defined as the ultimate global surface temperature change that would restore the energy balance at the top of the atmosphere, in response to an instantaneous doubling of carbon dioxide.

For HadGEM3.1-GC3.1-LL, the effective climate sensitivity is estimated to be 5.54 K [52], ranking the model used in the present study in the high end of climate models used in CMIP6, as far as the model's sensitivity to changes in carbon dioxide is concerned.

5.2. Time Series and Trends. In this section, the time series in the period from 2015 to 2100 of the components of the energy cycle are discussed for the SSP scenarios. In this respect, the time series of the four energy forms (*AZ*, *AE*, *KZ*, and *KE*, Figure 3), the four energy conversions ($<AZ \longrightarrow AE>$, $<AE \longrightarrow KE>$, $<KE \longrightarrow KZ>$, and $<AZ \longrightarrow KZ>$, Figure 4), and the available potential energy generation and the kinetic energy dissipation (*GZ*, *GE*, *DZ*, and *DE*, Figure 5) are presented. These graphs show the computed daily values of each energy cycle component in the period, with a corresponding linear regression equation superimposed.

5.2.1. Energy Contents. The time series for the four energy forms and for each of the SSP-based scenarios are shown in Figures 3(a)–3(c).

It appears that *AZ* tends to decrease over time under all SSP scenarios, with a tendency to become slightly more pronounced with increasing SSP forcing. *AE* also exhibits a negative trend, but the effect of the SSP forcing does not seem to yield appreciable differences between the different scenarios; other than that, the negative trend is slightly increased under the highest one.

The impact of different SSPs on *KZ* is easily identifiable: the trend in the time series of *KZ* exhibits an increase with time. Also, increasing forcing enhances the increasing trend of *KZ*, with the ssp585 scenario having the highest effect on the increasing trend: indeed, the increase in the *KZ* with time is quite notable under this latter scenario. This result is aligned with the findings from the energy balance analysis in Section 5.1, which has led to the inference that the increase in SSP forcing leads to an enhancement of the zonal wind field.

The time series of the other kinetic energy component, namely, *KE*, exhibits a different trend, which appears to be negative with all the SSP-based scenarios. This is interpreted as a tendency for weakening of the kinetic energy of the eddy motions with time.

5.2.2. Energy Conversions. The time series for the four energy conversions and for each of the SSP-based scenarios are shown in Figures 4(a)–4(c).

The time series for $<AZ \longrightarrow AE>$ exhibits a negative trend under all SSP-based scenarios, which is more pronounced under ssp585. This conversion term is always positive, irrespective of the level of SSP forcing, implying that the horizontal and vertical transfer of sensible heat is at all times towards lower temperature zones.

The trend of $<AE \longrightarrow KE>$ does not exhibit any appreciable change between different SSPs. Also, $<AE \longrightarrow KE>$ remains positive under all forcings, indicating the prevalence of rising of warmer air and sinking of colder air within latitude zones.

The trend in the conversion rates $<KE \longrightarrow KZ>$ does not exhibit any appreciable change between different SSPs. However, this conversion term occasionally attains negative values, albeit occurring at comparatively low rates; this finding suggests that the prevailing eddy transport of angular momentum is towards areas of higher angular velocity, thus feeding the zonal flow, but in some cases, this process reverses sign, and thus the kinetic energy of the eddies is enhanced at the expense of the zonal flow.

The conversion term between the two zonal components of energy, $<AZ \longrightarrow KZ>$, exhibits a negative trend under all SSP scenarios, which is more pronounced under ssp585. Nevertheless, it is worth noting the astounding alternating modes of this conversion term. As explained above, the conversion from *AZ* into *KZ* is accomplished by the sinking of colder air in colder latitude zones and rising of warmer air in warmer latitude zones. Indeed, as it was discussed in Section 5.1, this physical process leads, on average, to a conversion in the direction of enhancing the zonal flow at the expense of the zonal available potential energy, as postulated by Lorenz [2–4, 53]. However, the time series of $<AZ \longrightarrow KZ>$ suggests that the atmospheric engine can reverse its mode of operation for several successive days, converting *KZ* into *AZ*, and vice versa. The conversion rates in either direction can be of comparable magnitude (see also the minimum and maximum values of $<AZ \longrightarrow KZ>$ in Table 1). A similar behavior was noted by Michaelides [39].

5.2.3. Energy Generation and Dissipation. The time series for the available potential energy generation terms (*GZ* and *GE*) and for the kinetic energy dissipation terms (*DZ* and *DE*) for each of the SSP scenarios are displayed in Figures 5(a)–5(c).

The trend for *GZ* is noted to decrease with increasing SSP forcing, and the reverse is noted regarding the trend for *GE*; both trends are more pronounced with time in the case of the more enhanced forcing, ssp585. The generation of zonal available potential energy (*GZ*) is positive throughout the period under study, whereas generation of eddy available potential energy (*GE*) obtains both positive and negative values.

Available potential energy is generated by diabatic heating processes which involve the spatial correlation between diabatic heating and temperature (see expressions for *GZ* and *GE* in equation (C.4)). In the troposphere, this correlation tends to be positive, since on average, the tropical atmosphere receives more heat than it loses through radiation back to space and the polar atmosphere radiates more energy than it receives. In addition, at a given latitude, the correlation between diabatic heating and temperature can also be positive due to the tendency for precipitation and latent heat release which may occur primarily in rising warm air masses (as, for example, in tropical revolving storms and monsoon circulations). However, in areas where this correlation between diabatic heating and temperature is negative, diabatic heating acts towards destroying the existing temperature gradients; for example, desert areas undergo strong radiative cooling in comparison to their surroundings, as it is reflected in the net radiation budget at the top of the atmosphere. Also, the equatorial tropopause is far below its radiative equilibrium temperature, while in middle latitudes, temperatures at these levels are above radiative equilibrium [54]. Hence, in the lower stratosphere, diabatic heating functions as a sink of available potential energy. The same is true of the mesopause levels, where the summer pole is cold and the

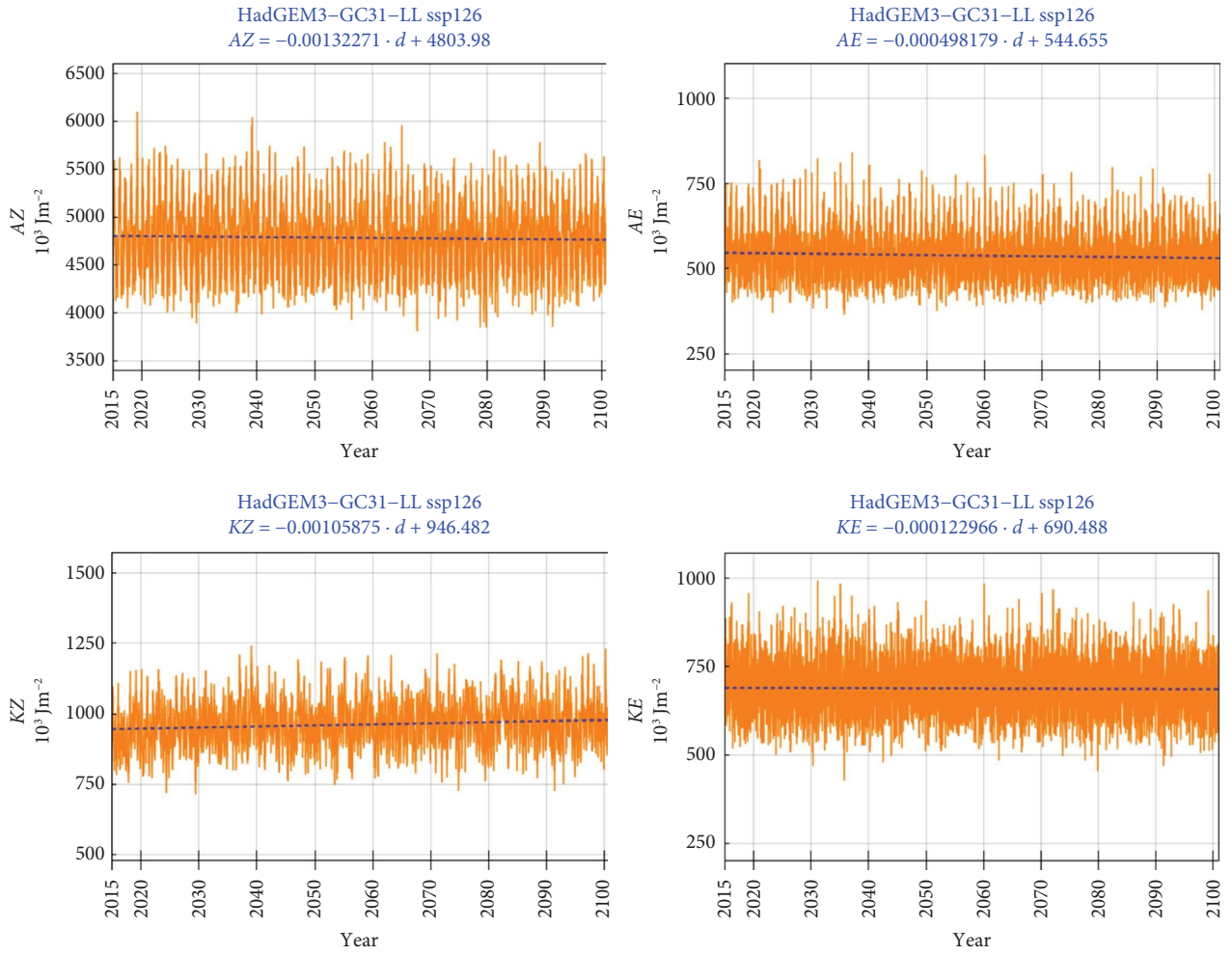

(a)

Figure 3: Continued.

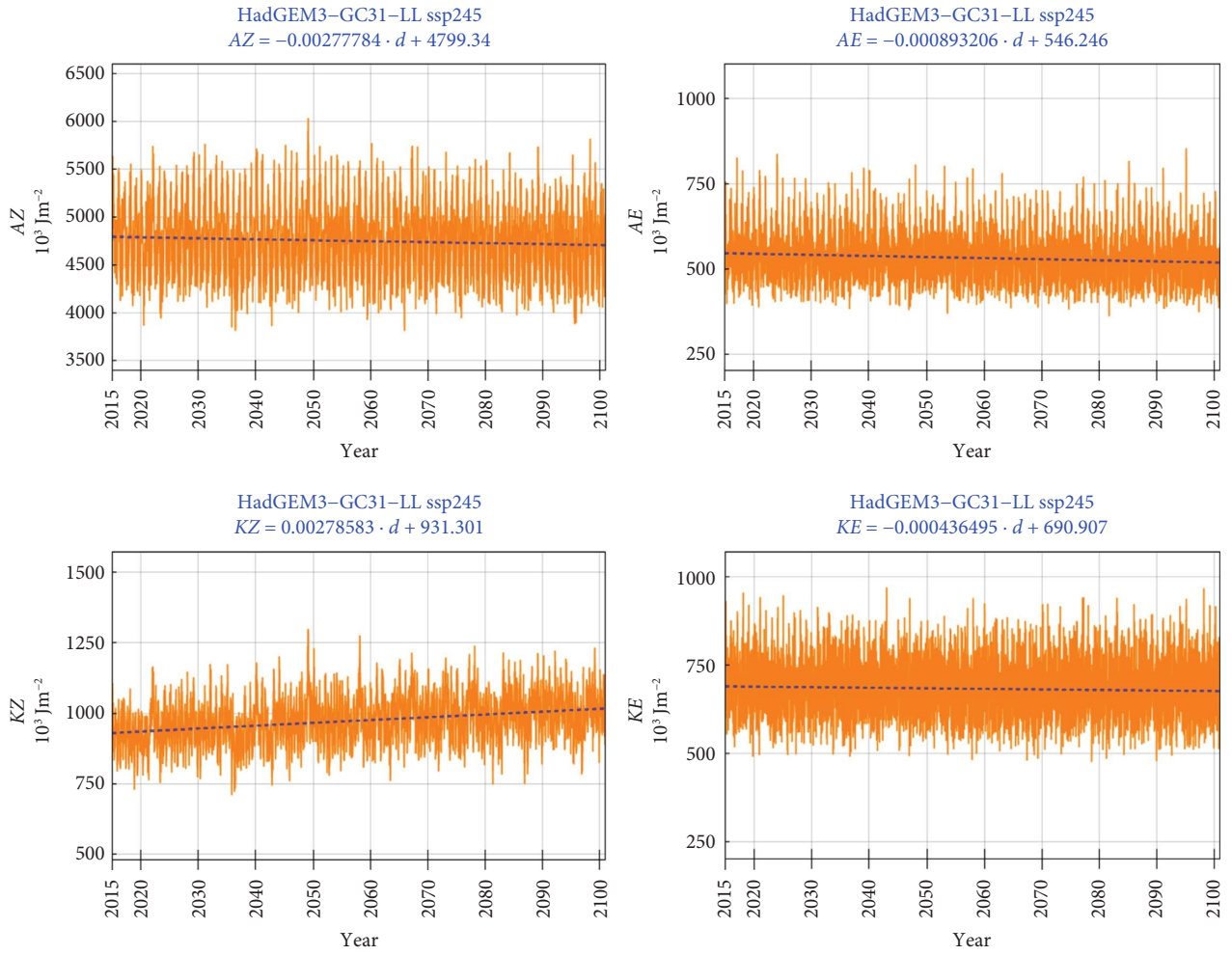

(b)

Figure 3: Continued.

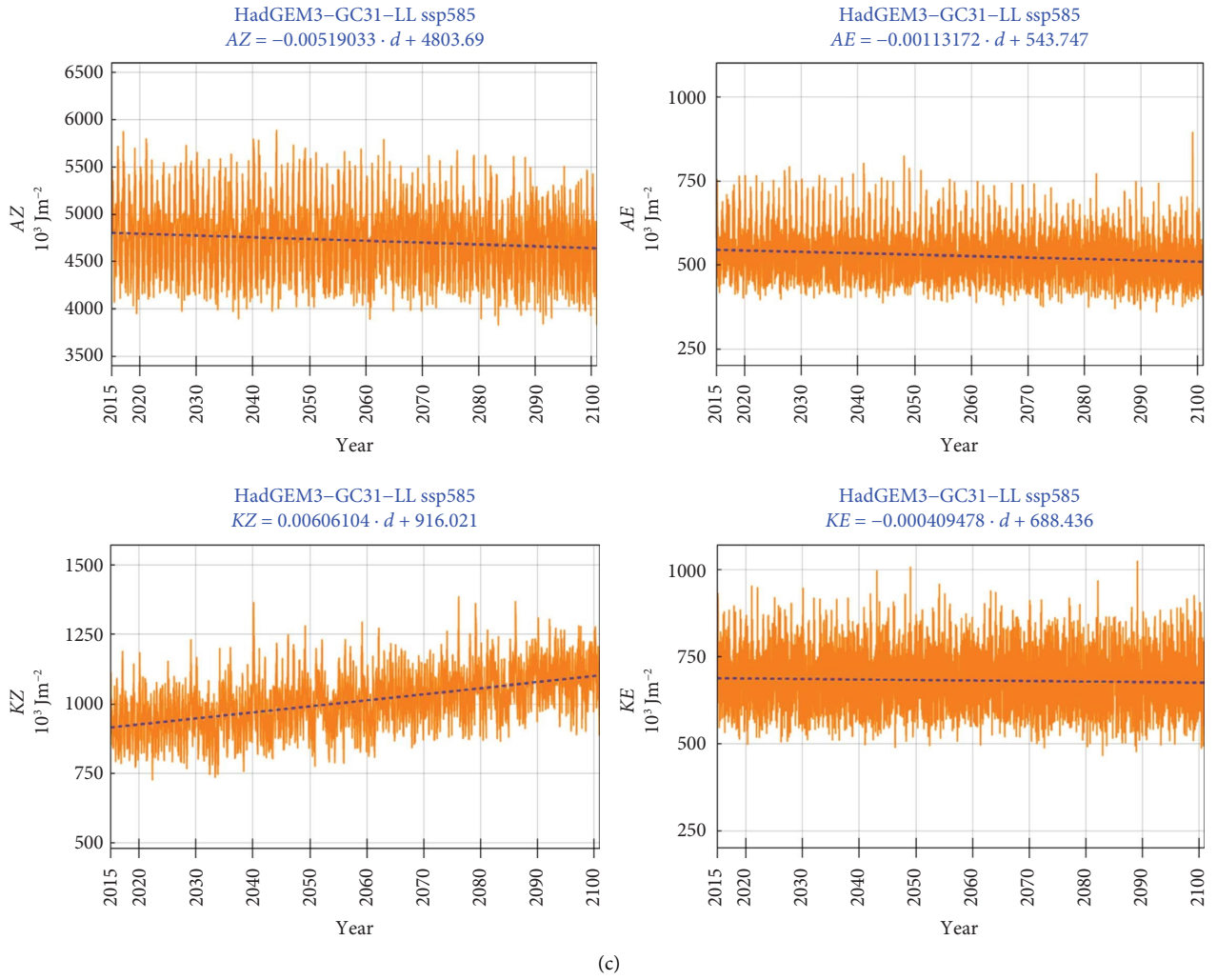

(c)

FIGURE 3: (a) Time series for energy forms for ssp126. The dashed line is the fitted linear regression which is given at the top of each diagram as a function of day (d). (b) Same as (a) but for ssp245. (c) Same as (a) but for ssp585.

winter pole is warm. From a thermodynamic point of view, these localized regions of the atmosphere function as refrigerators rather than as heat engines.

In a dry atmosphere, we would expect GE to be negative due to enhanced radiative cooling of warm anomalies, but in a moist atmosphere, condensation in the warm sectors of extratropical cyclones should favor positive GE generation.

The trend in DZ is not very much affected by the changing SSP scenario, but regarding the trend in DE, it tends to decrease more with increasing forcing.

5.3. Extremes in the Energy Components. In Table 1, the minimum and maximum values of the energetics components are displayed (for the energy contents, the values are in $10^3\,\mathrm{Jm}^{-2}$; for the energy conversion, generation, and dissipation, the values are in $10^{-3}\,\mathrm{Wm}^{-2}$). The presentation of these extreme values provides a framework for an appreciation of the extreme modes at which each of the components of the energy cycle may operate (though not necessarily occurring concurrently).

For AZ, its minimum values increase with increased SSP forcing, whereas for AE, the corresponding minimum values appear to decrease. Also, with increasing SSP forcing, the maximum values of AZ appear to decrease, whereas the maximum values of AE increase.

The maximum values of KZ at which the energy cycle operates increase with increasing forcing. Both the minimum and maximum values in KZ in the historical data are less than those in all the future SSP scenarios.

The highest maximum value of KE is reached with the highest forcing, ssp585, whereas with regard to the minimum values of KE, the situation is reversed, with the lowest minimum noted with the lowest forcing, ssp126.

The minimum in $<AZ \longrightarrow AE>$ falls below 50% in the largest forcing ssp585, compared to the lowest and medium ones. Both the maximum and minimum $<AZ \longrightarrow AE>$ in the historical data are notably higher than those in all the SSP-based scenarios.

The conversion of eddy energy, namely, $<AE \longrightarrow KE>$, behaves rather erratically in response to the increases in SSP forcing. The respective minima, however, exhibit a notable

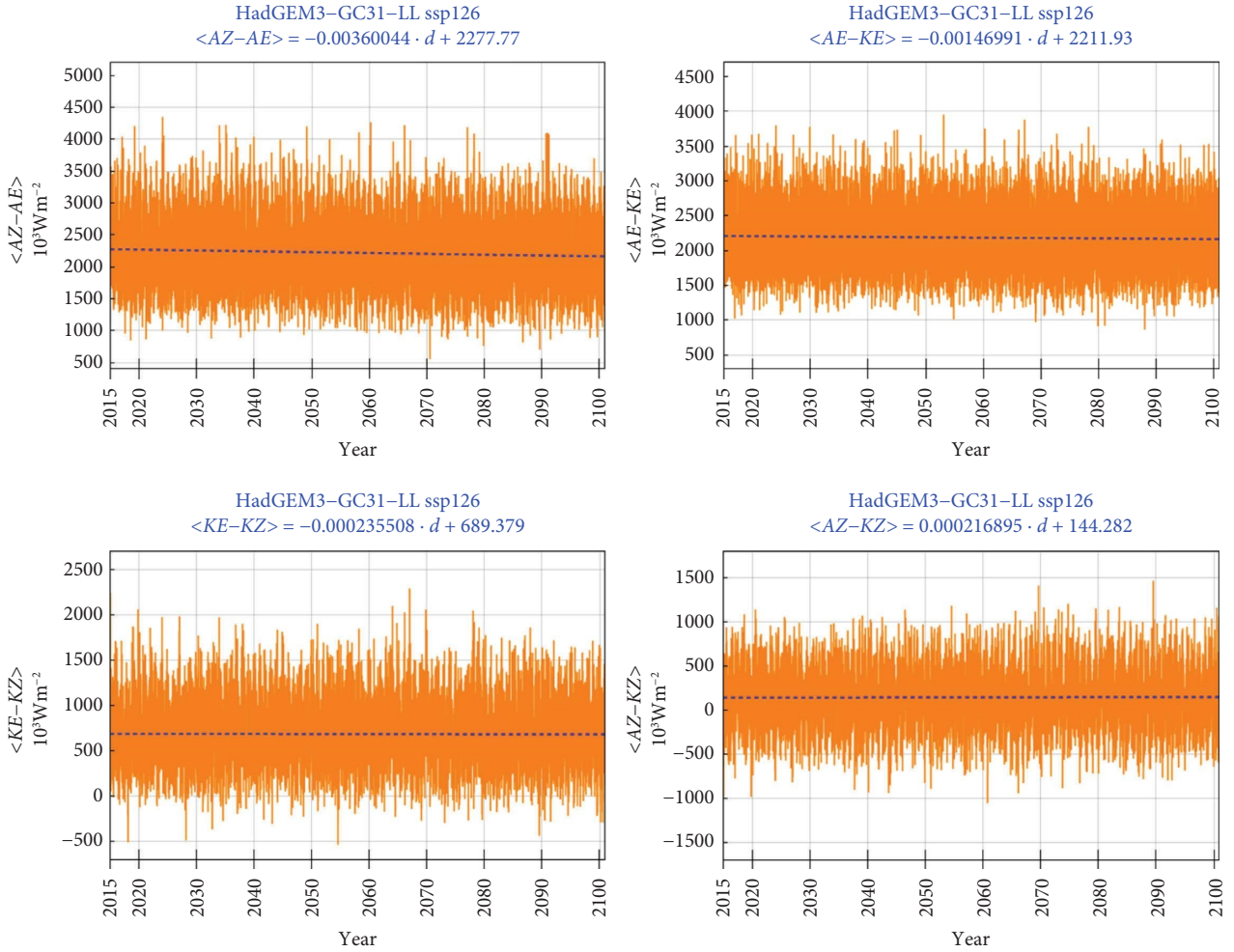

(a)

Figure 4: Continued.

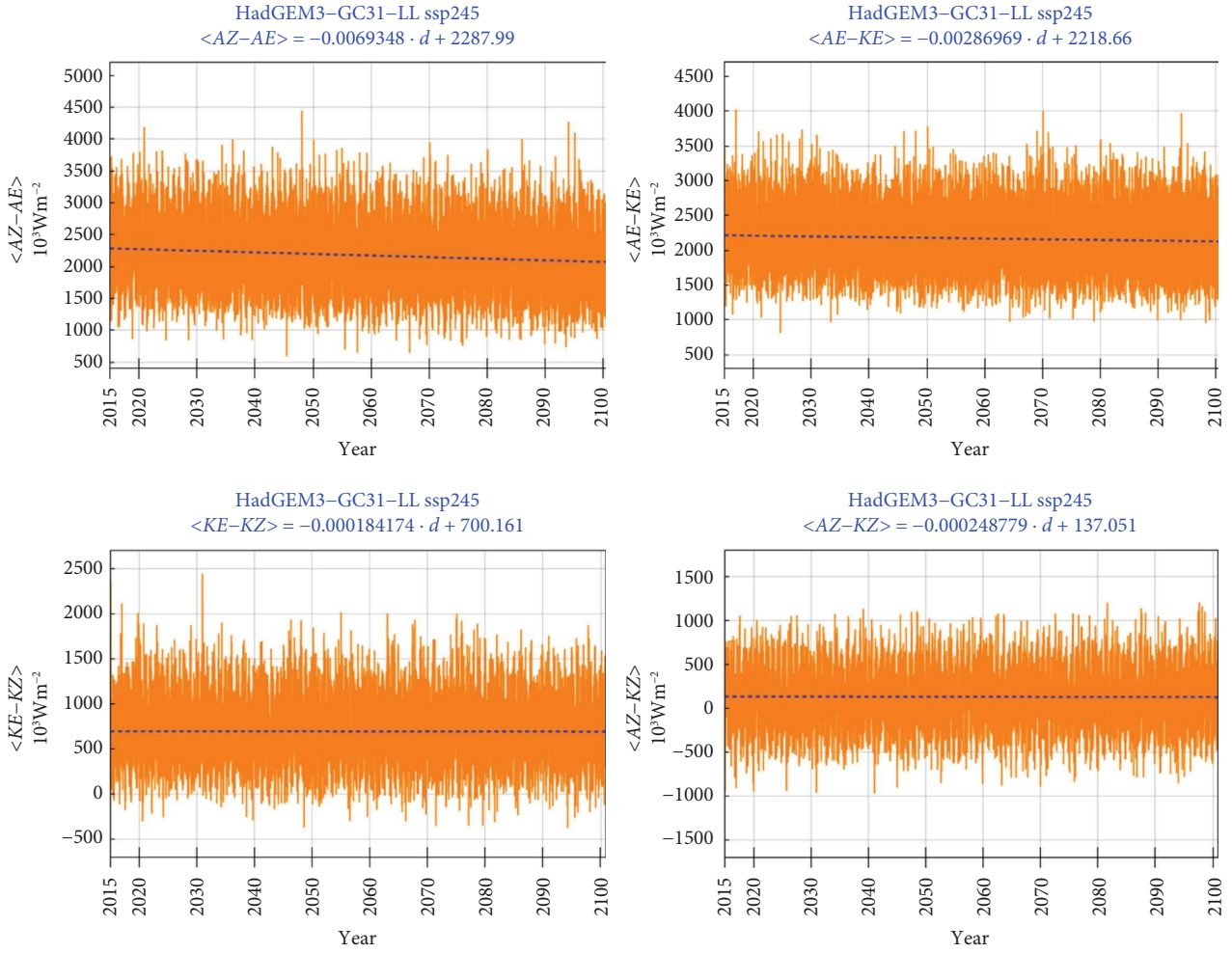

(b)

Figure 4: Continued.

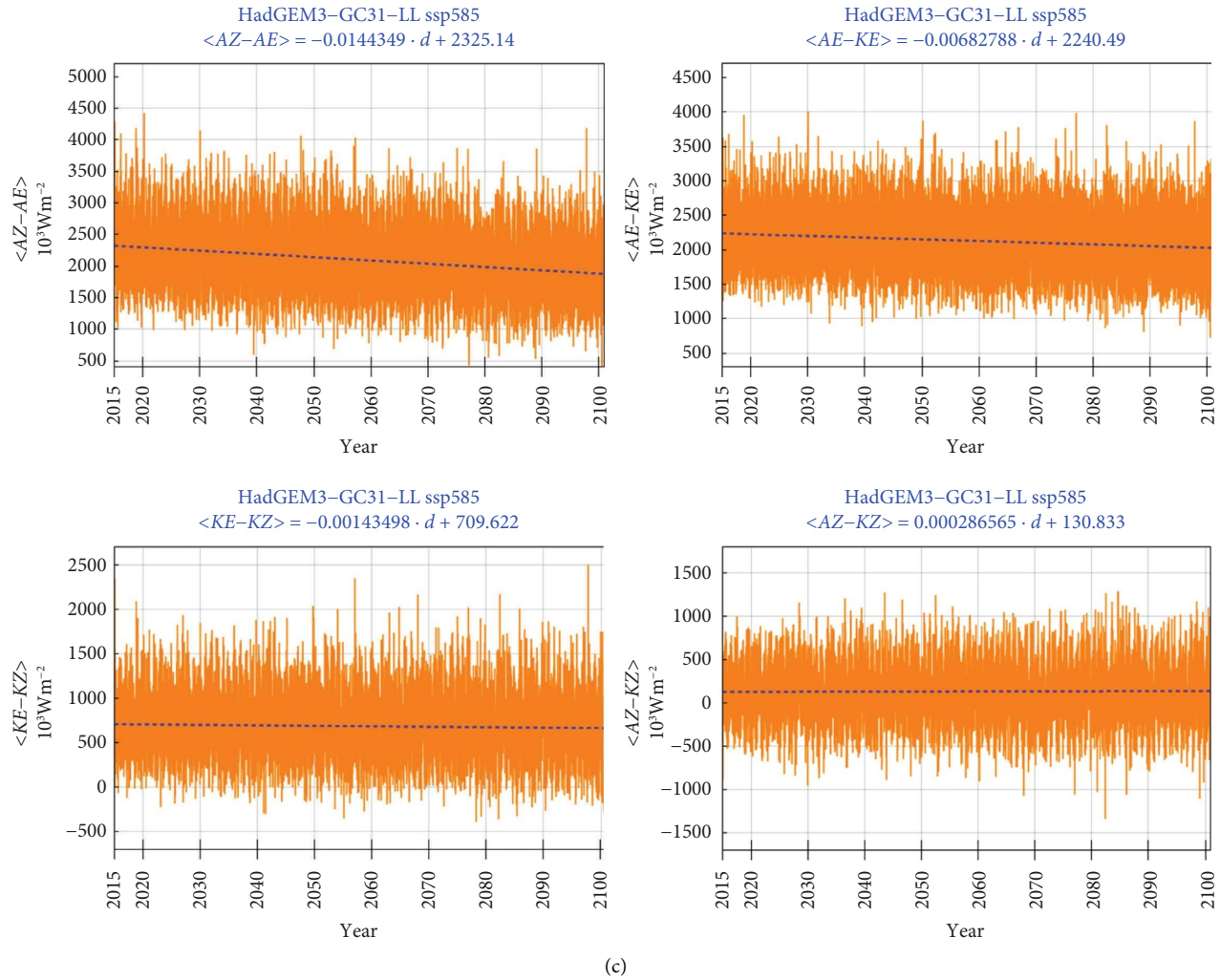

(c)

Figure 4: (a) Time series for energy conversions for ssp126. The dashed line is the fitted linear regression which is given at the top of each diagram as a function of day (d). (b) Same as (a) but for ssp245. (c) Same as (a) but for ssp585.

Table 1: Energy contents, conversion, generation, and dissipation terms.

	ssp126		ssp245		ssp585		Historical	
	Min	Max	Min	Max	Min	Max	Min	Max
AZ	3809	6106	3814	6041	3828	5898	3805	6001
AE	364	841	361	854	358	897	369	866
KZ	715	1243	711	1299	725	1389	661	1197
KE	428	994	476	972	465	1027	476	1016
$\langle AZ \longrightarrow AE \rangle$	553	4354	595	4447	216	4428	759	4886
$\langle AE \longrightarrow KE \rangle$	866	3954	816	4028	726	4015	763	4432
$\langle KE \longrightarrow KZ \rangle$	−539	2295	−378	2449	−392	2508	−617	2250
$\langle AZ \longrightarrow KZ \rangle$	−1054	1474	−971	1210	−1341	1296	−891	1235
GZ	79.8148	4421.31	−88.3889	4362.22	−12.5	4051.41	−195.833	4412.04
GE	−1047.04	965.667	−927.407	986.37	−985.241	1135.13	−1154.98	719.778
DZ	208.778	1552.5	210.574	1579.94	214.852	1635.81	168	1154.98
DE	667.63	2384.13	772.537	2463.11	748.444	2385.06	859.204	2487.72

Units: energy contents in $10^3\,\mathrm{Jm}^{-2}$; energy conversion, generation, and dissipation in $10^{-3}\,\mathrm{Wm}^{-2}$.

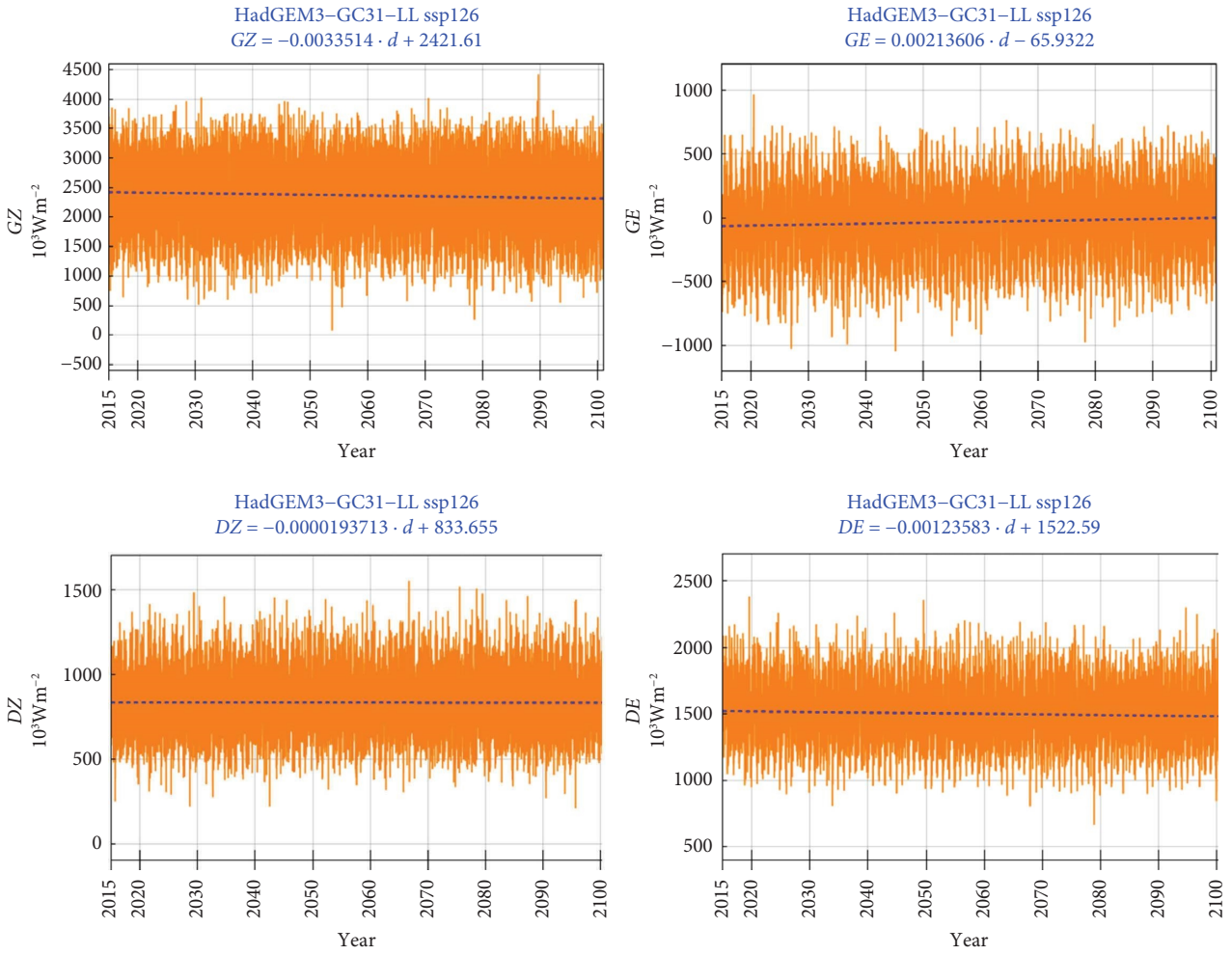

(a)

Figure 5: Continued.

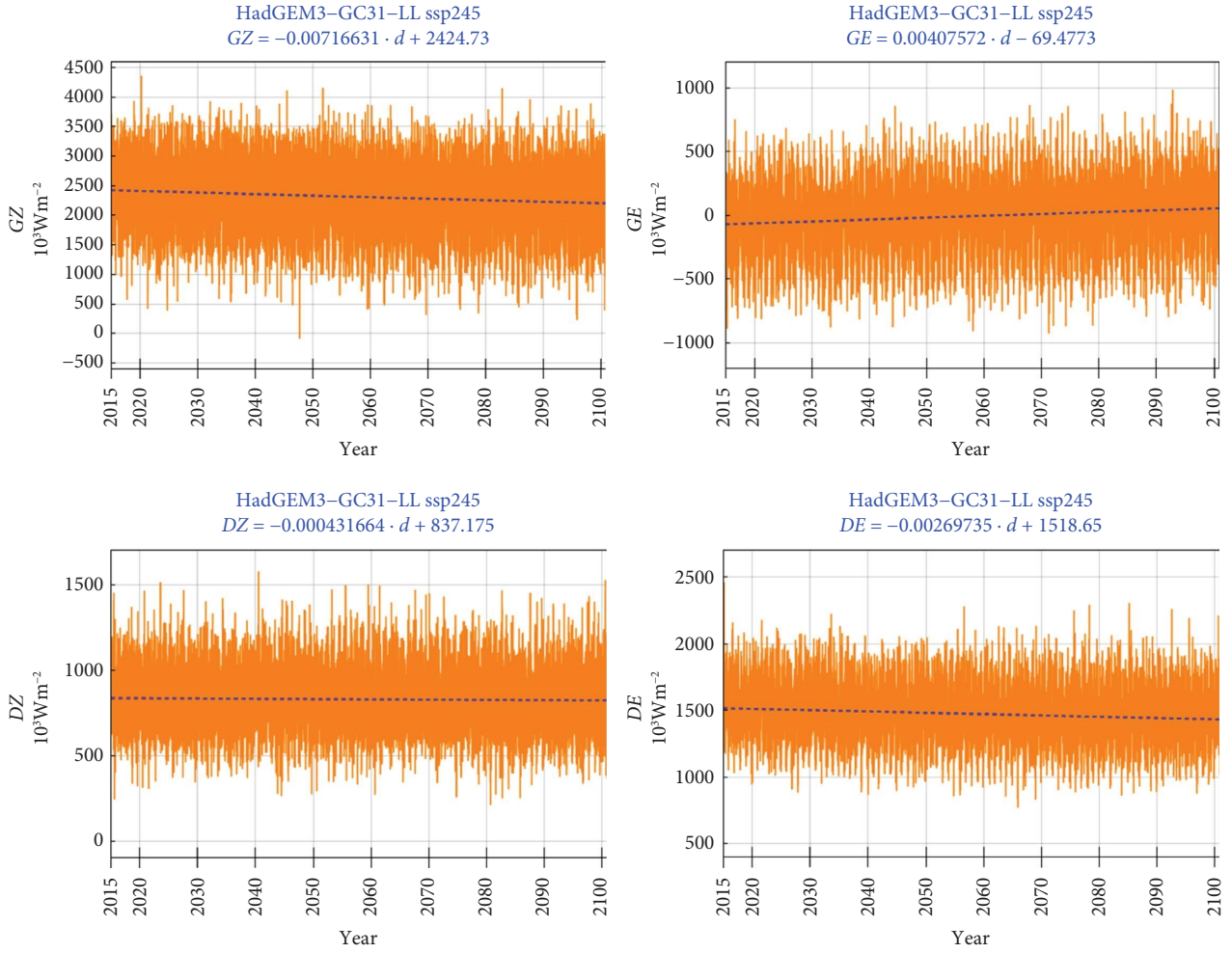

(b)

Figure 5: Continued.

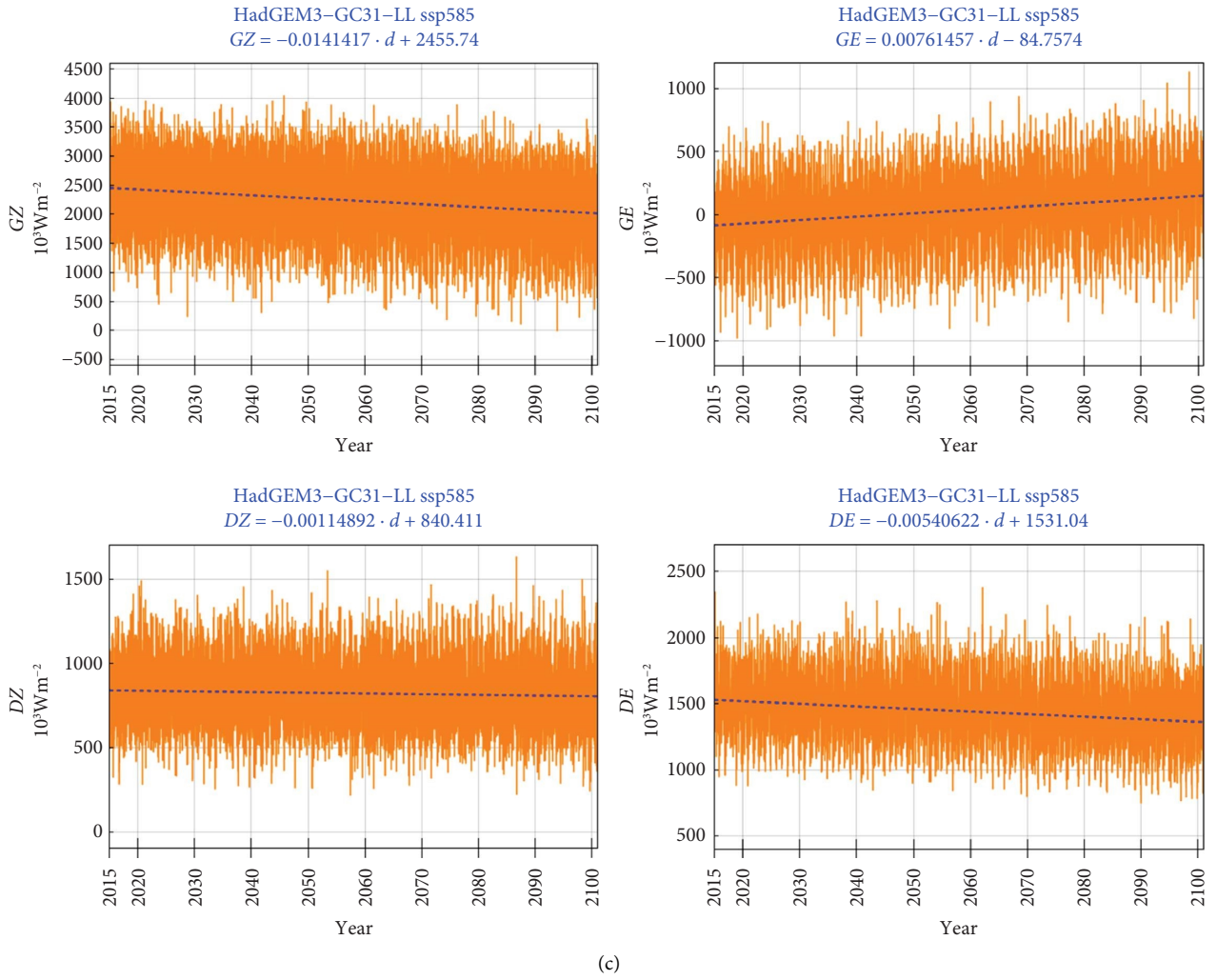

(c)

FIGURE 5: (a) Energy generation and dissipation for ssp126. The dashed line is the fitted linear regression which is given at the top of each diagram as a function of day (d). (b) Same as (a) but for ssp245. (c) Same as (a) but for ssp585.

decrease from their values under the ssp126 scenario to their corresponding values under the ssp585 scenario.

The conversion $<AZ \longrightarrow KZ>$ obtains its highest maximum values with the lowest forcing scenario. All the minimum values have a negative sign. From a closer examination of the values of this conversion term, as they have been calculated for each day (but also from examining the respective time series for this conversion rate in Figure 4, presented under Section 5.2.2), it was found that this term obtains negative values quite frequently and this reversal in behavior usually lasts for several consecutive days each time; this result implies that the respective underlying process can quite frequently and for several consecutive days operate in a reverse mode than what is anticipated on average and is based on Lorenz's postulations. To this end, the role of the Ferrel cell overturning atmospheric air is reiterated, as this meridional circulation is mostly responsible for the conversion of zonal available potential energy into zonal kinetic energy.

The conversion rate $<KE \longrightarrow KZ>$ is also found to obtain negative values, but this reversal in operation is quite rare (see also discussion in Section 3.2). The range of maximum values associated with changes in the forcing is quite small.

The maximum values of the generation term GZ exceed $4000 \times 10^{-3}\,\mathrm{Wm}^{-2}$, under all scenarios, representing the highest rates calculated in the energy cycle. Regarding the minima in GZ, it is noted that they embrace negative values, under the ssp245 and ssp585 scenarios; also, an outstanding negative minimum value is noted.

The highest maximum values for GE amount to about one-fourth of those for its GZ counterpart. The minimum values for GE are negative under all scenarios and the historical data.

The negative values obtained for GZ and GE (see also the series in Figures 5(a)–5(c)) are interpreted as a negative generation of available potential energy (by the diabatic processes involved). It is worth noting at this point that such negative generation of available potential energy was

calculated by Oort [23] even with time averaging on a hemispherical scale for *GE*. In the present research, such negative generation terms are explained by considering that the residual approach adopted here can lead to a temporary negative generation of available potential energy. However, as has been discussed in Section 5.1, under all scenarios, the overall (average) values for *GZ* are positive, whereas *GE* can become negative for the ssp126 and ssp245 scenarios.

The frictional forces are expected to dissipate kinetic energy; in line with this postulation, the minimum and maximum values of both the kinetic energy dissipation rates, *DZ* and *DE*, obtain positive values for all the SSP scenarios and the historical data. Increases in SSP forcing result in an increase in both the minimum and maximum values of *DZ*. Compared to all the SSP scenarios, the historical data reveal weaker minimum and maximum operation modes in *DZ* but stronger ones in *DE*.

5.4. Rate of Working: Efficiency of Energy Conversion. Contemplating that the atmospheric climate system operates as a heat engine, Boer and Lambert [5] performed an analysis of Lorenz energetics based on model data and compared the findings to corresponding reanalysis-based estimates. This comparison between the energetics under "observed" and "simulated" conditions would yield an approach to objectively assess the differences in the "rate of working" of the atmospheres corresponding to different models. Indeed, in his study that makes use of 12 models participating in AMIP2, Gleckler [55] concluded that the overall "rate of working" of the model atmospheres was, on average, about 17% more vigorous than the average of the reanalysis-based estimates. It is not feasible to perform a comparison of the future model-based energetics calculations of this study against observation-based ones that would refer to the same time period: the calculations presented here refer to the period from 2015 to 2100, for most part of which no observational data are available. Along the line proposed by Boer and Lambert [5], however, the three SSP-based energetics calculations in this study can be contrasted to the respective historical-based energetics.

Within the framework of Lorenz's energy cycle, as discussed above, diabatic heating processes lead to available potential energy generation, namely, *AZ* and *AE*, at rates *GZ* and *GE*, respectively. The rates of adiabatic conversions from these forms of available potential energy into their kinetic energy counterparts (i.e., *KZ* and *KE*) are accomplished at rates $<AZ \longrightarrow KZ>$ and $<AE \longrightarrow KE>$. In addition to these conversions, however, in Lorenz's energy cycle, two more energy conversions are also accomplished at rates $<AZ \longrightarrow AE>$ and $<KE \longrightarrow KZ>$. Lastly, kinetic energy is dissipated by frictional processes into heat (at rates *DZ* and *DE*). Bearing in mind these considerations, changes in the "rate of working" of the climate system could be assessed via the changes in the rates at which energy is generated (energy generation rate of working), converted (energy conversion rate of working), and dissipated (energy dissipation working rate) (see [39]). In this paper, the rate of working of the atmospheric heat engine is contemplated in terms of the directly calculated energy conversions, $<AZ \longrightarrow AE>$, $<AE \longrightarrow KE>$, $<KE \longrightarrow KZ>$, and $<AZ \longrightarrow KZ>$.

Contrasting the energetics of the simulated future states of the atmosphere to the energetics of a state based on an independent observational dataset would be ideal in order to assess the changes in the efficiency of Lorenz energy cycle under different SSP scenarios against a baseline (see [5]). However, this is not feasible in this study, as explained above. An alternative to this is to assess the changes in the rates of working under different SSPs relative to the energetics of the atmosphere calculated on historical data; in this case, the baseline is founded on the historical dataset (from 1929 to 2014, having an 85-year time span which is the same as the climatic SSP projections, as explained in Section 3.1).

The percentage changes in the energy conversions under each of the SSP scenarios with respect to the baseline are displayed in Figure 6. With the exception of the percentage change in $<AZ \longrightarrow KZ>$ under ssp126, all the changes in efficiencies are negative. Therefore, it can be inferred that, generally speaking, the SSP forcing causes the energy conversion working rate to decrease in the future scenarios compared to the baseline. The change in the efficiency of the conversions of energy from *AZ* into *AE* and from *AE* into *KE* decreases with increasing forcing. On average, considering all the conversion terms, the energy conversion efficiency decreases from −2.51% under ssp126 to −5.21% under ssp245 and to −6.46% under ssp585.

6. Discussion

The Lorenz cycle of energy of the atmosphere has been used in numerous studies on the diagnosis of the atmospheric dynamics. The present study focuses on investigating whether different climate scenarios, as they have been adopted in the CMIP6 project, can lead to different regimes in the energetics components in Lorenz's energy cycle. It comes as no surprise that the results of the present study demonstrate that different future climate scenarios (as they are delineated by the CMIP6 simulations with the Hadley Centre's HadGEM3-GC3.1 model) have a diverse effect on the components of the Lorenz energy cycle. Boer [56] and Lucarini et al. [57] suggest that the warming of the atmosphere due to increased concentration of greenhouse gases, and specifically that of carbon dioxide, can lead to a smoothing of the meridional temperature gradients, subsequently reducing the availability of potential and internal energies for conversion into kinetic energy. This may explain the trend for a decrease of the available potential energy reservoirs with increasing gas concentrations, which is more notable for *AZ* than for *AE* (see Figures 2 and 3).

Both the energy balances (Figure 2) and the trends in the respective time series (Figure 5) denote a notable increase in *KZ* as a result of increasing SSP forcing. Since the meridional temperature gradient should be decreasing under future scenarios with increased gas concentrations, the thermal wind and subsequently the vertical wind shear should also be expected to decrease. Therefore, the current increases in *KZ* estimated under increased gas concentrations cannot be explained through baroclinic processes, but other barotropic

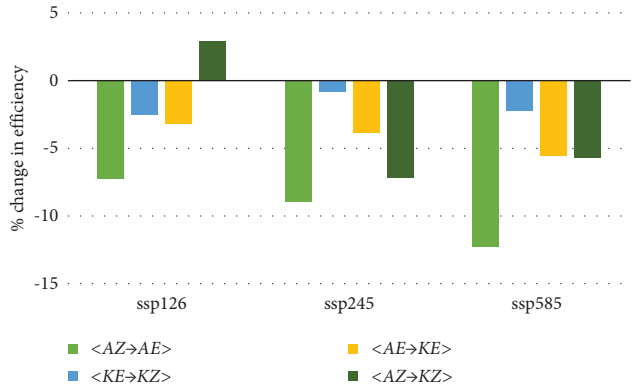

FIGURE 6: Change in efficiency of energy conversion under different SSPs, considering the historical data as a baseline.

processes should be at work in converting *AZ* into *KZ*. Such barotropic processes may be related to surface changes, as it has been proposed by Li et al., [45]. Indeed, using observational data, Li et al. [45] calculated the components of Lorenz's energy cycle in the period 1979–2001. They have concluded that the Ferrel cell-related conversion from zonal kinetic to zonal available potential energy (i.e., negative $<AZ \longrightarrow KZ>$ conversion) is bigger and stronger than the Hadley cell-related one (i.e., positive $<AZ \longrightarrow KZ>$ conversion); indeed, considering only the free tropospheric layer (above 700 hPa), the net estimate of $<AZ\text{-}KZ>$ is negative, i.e., leading to a conversion of *KZ* into *AZ*. However, they have noted considerably large positive conversion values in the near-surface parts (between 1000 and 700 hPa) of the Ferrel and the Polar cell, which are more notable in the Southern Hemisphere. Their findings suggest that near-surface processes play an important role in the positive conversion rate from *AZ* into *KZ* which can probably change the global direction of the conversion rate. In relation to the current analysis, the combined positive effect of these barotropic near-surface processes together with those of the Hadley cell could be more pronounced with increasing gas concentrations.

Regarding *KE*, however, the tendency is for the kinetic energy of the eddying motions to decrease with increasing forcing. These contradictory tendencies in the two kinetic energy components are partly dictated by the enhanced conversion from *KE* into *KZ*, i.e., $<KE \longrightarrow KZ>$, noted at the highest SSP forcings, ssp245 and ssp585. The physical interpretation of this increased $<KE \longrightarrow KZ>$ conversion rate is that the angular momentum transfer by the eddies towards the areas of higher angular velocity will lead to an enhancement of the zonal flow.

Boer [56] had performed simulations with changing carbon dioxide scenarios using the Canadian Climate Centre General Circulation Model. This investigation refers to Northern Hemisphere middle latitudes during wintertime and focused on the effects of doubling of carbon dioxide concentrations. The basic finding in regard to the intensity of the intensity of atmospheric energetics is that they are suppressed as the concentration increases. Also, Hernández-Deckers and von Storch [42] have performed simulations with the ECHAM5/MPI-OM model under different carbon dioxide regimes and presented their findings in regard to the effects on Lorenz energy cycle. The decrease in the efficiency of the atmospheric engine in converting available potential energy into kinetic energy as more greenhouse gases are accumulated into the atmosphere is claimed by these authors to be a consequence of the slackening of the meridional temperature gradient [42, 56]. Based on a study investigating the global warming impacts on the thermodynamics of the climate system, Lucarini et al. [57] concluded that as the climate becomes warmer, it features higher entropy production and also it becomes less efficient and more irreversible. In agreement with the above findings, in the present study, a tendency for the available potential energy to be converted into kinetic energy is reduced with increased SSP forcing, with this reduction being more notable with $<AE \longrightarrow KE>$; this implies a weakening of the sinking of colder air and rising of warmer air within the latitude zones.

The choice of the Hadley Centre's HadGEM3-GC3.1 model is just one of the models available under the CMIP6. In this paper, this version of the model was chosen in order to contrast the results with those in a previous study that were based on a predecessor model. In a recent study on CMIP5 data, Michaelides [39] had used the simulations from a previous version of the Hadley Centre climatic model, namely, HadGEM2-ES. In the current study, the choice of the Hadley Centre's HadGEM3-GC3.1 model available within the framework of the CMIP6 was purposedly made in an effort to make some comparative remarks on the energy cycle between the two most recent model intercomparison projects. Although the results cannot be strictly compared, primarily because the CMIP5 simulations are based on the RCP scenarios, whereas the CMIP6 are based on the SSP ones, some general comments are made in the following. As explained in Section 1, the ssp126, ssp245, and ssp585 scenarios adopted in the present study embrace the RCP2.6, RCP4.5, and RCP8.5 global forcing pathways used in the study in [39], respectively. Contrasting the results from the corresponding SSP and RCP scenarios (i.e., Figure 2 in this study and Figure 2 in [39]), it is clear that the strength of the Lorenz energy cycle is notably larger in the present study than that of the previous one. In an effort to explain the differences in the results of the two studies, the inherent characteristics of the two datasets are contrasted. The horizontal spatial resolution of the two datasets is the same (latitude 1.25° and longitude 1.875°); also, the time step in the output storage of the two datasets is the same (24 hours). However, the two datasets differ with regard to their vertical resolution. Indeed, in the CMIP5 simulations, the vertical resolution in the data refers to eight isobaric levels with the top one being at 10 hPa, whereas in the CMIP6 simulations, the vertical resolution of the data is at nineteen pressure levels with the top one being at 1 hPa. Apparently, the resolution in the vertical is denser in the CMIP6 data; also, the CMIP6 data reflect on an atmosphere that is deeper than that of the CMIP5; therefore, with the CMIP6, the numerical calculations of the vertical integrals (see Appendix C) are performed over a deeper atmospheric layer compared to the calculations with the CMIP5 data [39].

To the best of the author's knowledge, no other study has been performed on the energetics of Lorenz cycle by using simulations from models participating in the CMIP6 project. However, two studies on the energetics of the atmosphere that make use of data from the CMIP5 project are those by Veiga and Ambrizzi [58] and Michaelides [39] who have studied the effect of different RCPs on Lorenz energy cycle. Comparing the energy balances of the present study to those in the study by Veiga and Ambrizzi [58], it can be seen that the conversion terms are in good agreement. The same is noted regarding all the energy contents but the zonal available potential energy. In the study in hand, AZ was found to have much larger values. In fact, in the present study, the comparison of AZ contents and AE contents reveals that the former is almost nine times the latter, whereas in the study by Veiga and Ambrizzi [58], the values of both zonal and eddy available potential energy contents are very close.

In general, the conversion terms are higher in the present study compared to those of Michaelides [39]. Regarding $<AZ \longrightarrow KZ>$, there is a general agreement regarding the impact of enhanced forcing on this conversion rate in both the present study and that of Michaelides [39]: in both studies, this conversion decreases with increasing forcing. The same decrease in $<AZ \longrightarrow AE>$ with increasing forcing is also noted in both studies. The impact of increased forcing on the conversion between the eddy components of available potential and kinetic energies, i.e., $<AE \longrightarrow KE>$, is in good agreement in both studies too.

At this point, it is worth noting some of the difficulties and limitations in establishing firm results by using an approach that is based on the energy cycle applied to climatic projections and the endeavor to calculate its components numerically.

The fundamental concept of the available potential energy in the energy cycle is defined over the entire atmosphere, and hence its application on local or regional scales entails a number of limitations. However, Muench [18, 19] considered the amount of available potential energy calculated over a limited atmospheric region as its contribution to the total available potential energy of the entire atmosphere, and he reformulated the energetics integrals to take into account boundary transfers of energy (see also [20, 40, 41]). Also, Marquet [59] discusses limitations that should be borne in mind when the concepts of energy and energy conversions are considered over a limited area.

Among the complications inherent in exploiting the Lorenz energy cycle concepts, one must take into consideration the necessary numerical solutions to the mathematical formulations that are adopted in order to carry out the calculations with the available atmospheric data.

Uncertainties are also intrinsic in future climate projections, stemming from a number of different sources that embrace the modelling process but also the forcings reflecting on the different socioeconomic assumptions, among others. As discussed in [60], one way to study uncertainty is through contemplating the results from multiple models, based on the implicit assumption that multiple models provide additional and more reliable information than a single model. A collection of results based on different climatic models could prove more appropriate rather than those from a single model. The motivation behind such a combination of results from multiple models can lead to an increased trustworthiness in the findings. This is planned to be the basis for a future study on the climatic projections of the energetics of the atmosphere. It should be anticipated, however, that differences in the energy cycle calculated with different sets of data from models participating in CMIP6 should exist. Indeed, differences between the models used in CMIP6 series of experiments could result in different projections (see [61–63]). These differences in the model projections will be reflected in the energetics analyses which will be based on them. To mitigate the deviations between the various models' energetics analyses, the data from all the models that will be used in such an endeavor should cover the same time period (so that the comparison is meaningful) but also have the same spatiotemporal characteristics (i.e., data frequency and horizontal and vertical resolution).

Appendix

A. List of Symbols

AE: eddy available potential energy

AZ: zonal available potential energy

c_p: specific heat of dry air for constant pressure

DE: dissipation of eddy kinetic energy

DZ: dissipation of zonal kinetic energy

F_λ: eastward component of kinetic energy dissipation

F_φ: northward component of kinetic energy dissipation

g: acceleration of gravity

GE: diabatic generation of eddy available potential energy

GZ: diabatic generation of zonal available potential energy

KE: eddy kinetic energy

KZ: zonal kinetic energy

p: atmospheric pressure

Q: diabatic processes leading to generation of available potential energy

R: gas constant for dry air

t: time

T: thermodynamic temperature

u: eastward component of velocity

v: northward component of velocity

σ: static stability

ω: Lagrangian pressure tendency

$<AE \longrightarrow KE>$: conversion of AE into KE

$<AZ \longrightarrow AE>$: conversion of AZ into AE

$<AZ \longrightarrow KZ>$: conversion of AZ into KZ

$<KE \longrightarrow KZ>$: conversion of KE into KZ

$[\bullet]_\lambda$: zonal average of a variable

$(\bullet)_\lambda$: departure from zonal average of a variable

$[\bullet]_{\lambda\varphi}$: area average of a variable

$([\bullet]_\lambda)_\varphi$: zonal average minus area average of variable

$R\,[\bullet]$: estimation of a variable as a residual

B. Numerical Analogues for Mathematical Computations

An orthogonal spherical coordinate system is adopted, where the horizontal components are λ (longitude) and φ (latitude); the vertical component is p (pressure).

Given that the grid distance in the dataset is 1.875° in the west-east and 1.25° in the south-north direction, respectively, the numerical computations are carried out on a (horizontal) global grid of 192×144 points, which are evenly distributed.

A zonal average of a quantity (X) is calculated as

$$[X]_\lambda = \frac{1}{2\pi}\int_0^{2\pi} X \mathrm{d}\lambda, \tag{B.1}$$

where the averaging is taken over an entire latitude circle. However, in the original CMIP6 dataset, some values of all the variables are shown as Not a Number (*NaN*) in the lowest atmospheric levels because of the protrusion of elevated land into these levels (from an examination of the data, this land masking is not fixed but varies with time). Apparently, these *NaN* "values" reflect values below the Earth's surface (i.e., where the surface pressure is lower than the nominal level pressure) and must not be used in the calculations; this fact is taken into consideration in the numerical solution of the above relationship by disregarding the grid points assigned a *NaN* in the numerical analogue of the above relationship, as the mass of the corresponding grid cells is zero.

The numerical analogue of equation (B.1) that has been used in the present calculations takes the form

$$[X]_\lambda = \frac{1}{2\pi}\sum_\lambda X \delta\lambda, \tag{B.2}$$

where $\delta\lambda$ is the grid distance in the longitudinal sense.

As mentioned above, because the original raw data contain values which are denoted as *NaN* (Not a Number), in the numerical calculations, care must be taken into account in averaging.

$$[X]_\lambda = \frac{\sum_\lambda X \cos\varphi\, \delta\lambda}{2\pi - \sum_k \delta\lambda}, \tag{B.3}$$

where the summation (k) in the denominator is taken over all grid points that are assigned a *NaN* "value" in the raw data retrieved.

The departure from the above zonal average calculated at every grid point is defined as

$$(X)_\lambda = X - [X]_\lambda. \tag{B.4}$$

An area average is defined as follows, where r is the mean radius of the Earth

$$[X]_{\lambda\varphi} = \frac{1}{4\pi r^2}\int_{-\pi/2}^{\pi/2}\int_0^{2\pi} X r^2 \cos\varphi \mathrm{d}\lambda\, \mathrm{d}\varphi. \tag{B.5}$$

Bearing in mind the above, the numerical analogue that was used herein in order to calculate the area average is given by

$$[X]_{\lambda\varphi} = \frac{\sum_\varphi \sum_\lambda X \cos\varphi\, \delta\lambda\delta\varphi}{4\pi - \sum_k \cos\varphi_k \delta\lambda\delta\varphi}, \tag{B.6}$$

where the summation (k) in the denominator is taken over all grid points that are assigned a *NaN* "value" in the raw data retrieved.

Lastly, a quantity as defined by the following equation is calculated:

$$([X]_\lambda)_\varphi = [X]_\lambda - [X]_{\lambda\varphi}. \tag{B.7}$$

The horizontal and vertical derivatives are numerically evaluated using a finite difference approach. For the vertical integrals, a trapezoidal rule is adopted.

C. Integral Expressions for Energetics Components

Vertical integration is performed stepwise throughout the atmospheric layers defined by the 19 atmospheric layers explained in Section 3.1. The upper and lower pressure levels are denoted by p_1 and p_2 ($p_1 < p_2$).

The four energy forms are given by the following mathematical expressions:

$$\begin{aligned} AZ &= \int_{p_1}^{p_2} \frac{\left[\left([T]_\lambda\right)_\varphi^2\right]_{\lambda\varphi}}{2[\sigma]_{\lambda\varphi}} \mathrm{d}p, \\ AE &= \int_{p_1}^{p_2} \frac{\left[(T)_\lambda^2\right]_{\lambda\varphi}}{2[\sigma]_{\lambda\varphi}} \mathrm{d}p, \\ KZ &= \int_{p_1}^{p_2} \frac{\left[(u)_\lambda^2 + (u)_\lambda^2\right]_{\lambda\varphi}}{2g} \mathrm{d}p, \\ KE &= \int_{p_1}^{p_2} \frac{\left[[u]_\lambda^2 + [v]_\lambda^2\right]_{\lambda\varphi}}{2g} \mathrm{d}p, \end{aligned} \tag{C.1}$$

where T is thermodynamic temperature, u and v are the eastward and northward wind components (in $\mathrm{m{\cdot}s^{-1}}$), and σ is a static stability parameter (in $\mathrm{K^2 m^{-1}}$) defined by

$$\sigma = \frac{gT}{c_p} - \frac{pg}{R}\frac{\partial T}{\partial p}, \tag{C.2}$$

where g is the global average of the gravitational acceleration ($9.81\ \mathrm{m{\cdot}s^{-2}}$), c_p is the specific heat of air for constant pressure, and R is the gas constant for dry air.

The four energy conversion terms are given by

$$\langle AZ \longrightarrow KZ\rangle = \int_{p_1}^{p_2} -\left[\left([T]_\lambda\right)_\varphi \left([\omega]_\lambda\right)_\varphi\right]_{\lambda\varphi} \frac{R}{gp}\,\mathrm{d}p,$$

$$\langle AE \longrightarrow KE\rangle = \int_{p_1}^{p_2} -\left[(T)_\lambda\,(\omega)_\lambda\right]_{\lambda\varphi} \frac{R}{gp}\,\mathrm{d}p,$$

$$\langle AZ \longrightarrow AE\rangle = \int_{p_1}^{p_2} -\left(\left[\frac{(T)_\lambda\,(v)_\lambda}{2[\sigma]_{\lambda\varphi} r} \frac{\partial\left([T]_\lambda\right)_\varphi}{\partial\varphi}\right]_{\lambda\varphi} + \left[\frac{(T)_\lambda\,(\omega)_\lambda}{p^{R/c_p}} \frac{\partial}{\partial p}\left(\frac{\left([T]_\lambda\right)_\varphi p^{R/c_p}}{[\sigma]_{\lambda\varphi}}\right)\right]_{\lambda\varphi}\right)\mathrm{d}p,$$

$$\langle KE \longrightarrow KZ\rangle = \int_{p_1}^{p_2} \frac{1}{g}\left(\left[\frac{\cos\varphi}{r}(u)_\lambda\,(v)_\lambda \frac{\partial}{\partial\varphi}\left(\frac{[u]_\lambda}{\cos\varphi}\right)\right]_{\lambda\varphi} + \left[\frac{(v)_\lambda^2}{r} \frac{\partial[v]_\lambda}{\partial\varphi}\right]_{\lambda\varphi} + \left[\frac{\tan\varphi}{r}(u)_\lambda^2[v]_\lambda\right]_{\lambda\varphi} + \left[(\omega)_\lambda\,(u)_\lambda \frac{\partial[u]_\lambda}{\partial p}\right]_{\lambda\varphi} + \left[(\omega)_\lambda\,(v)_\lambda \frac{\partial[v]_\lambda}{\partial p}\right]_\varphi\right)\mathrm{d}p. \tag{C.3}$$

The energy generation and dissipation terms are given by

$$GZ = \int_{p_1}^{p_2} \frac{\left[\left([T]_\lambda\right)_\varphi \left([Q]_\lambda\right)_\varphi\right]_{\lambda\varphi}}{c_p\,[\sigma]_{\lambda\varphi}}\,\mathrm{d}p,$$

$$GE = \int_{p_1}^{p_2} \frac{\left[(T)_\lambda\,(Q)_\lambda\right]_{\lambda\varphi}}{c_p\,[\sigma]_{\lambda\varphi}}\,\mathrm{d}p,$$

$$DZ = \int_{p_1}^{p_2} \frac{1}{g}\left[[u]_\lambda\left[F_\lambda\right]_\lambda + [v]_\lambda\left[F_\varphi\right]_\lambda\right]_{\lambda\varphi}\mathrm{d}p, \tag{C.4}$$

$$DE = \int_{p_1}^{p_2} \frac{1}{g}\left[(u)_\lambda\,(F_\lambda)_\lambda + (v)_\lambda\left(F_\varphi\right)_\lambda\right]_{\lambda\varphi}\mathrm{d}p,$$

where Q denotes the diabatic processes leading to generation of APE and F_λ and F_φ are the eastward and northward components of friction, respectively.

D. Estimation of Energy Generation and Dissipation Terms as Residuals

The quantities GZ, GE, DZ, and DE are estimated as residuals in the respective energy balance equations, as follows:

$$R[GZ] = \frac{\partial AZ}{\partial t} + \langle AZ \to KZ\rangle + \langle AZ \to AE\rangle,$$

$$R[GE] = \frac{\partial AE}{\partial t} - \langle \mathrm{AZ} \to AE\rangle + \langle AE \to KE\rangle,$$

$$R[DZ] = -\frac{\partial KZ}{\partial t} + \langle KE \to KZ\rangle + \langle AZ \to KZ\rangle, \tag{D.1}$$

$$R\,[DE] = -\frac{\partial KE}{\partial t} + \langle AE \to KE\rangle - \langle KE \to KZ\rangle.$$

The above partial derivatives of the four energy forms denote tendencies with respect to time (t).

Data Availability

The data used in this study are freely available from the Earth System Grid Federation (ESGF).

Conflicts of Interest

The author declares that there are no conflicts of interest.

Acknowledgments

This work was supported by the EMME-CARE project that received funding from the European Union's Horizon 2020 research and innovation programme under grant agreement no. 856612 and the Cyprus Government. The World Climate Research Programme, through its Working Group on Coupled Modelling, coordinated and promoted CMIP6 and it is hereby acknowledged. Also, the author wishes to extend his thanks to the climate modelling groups for producing and making available their model output, the Earth System Grid Federation (ESGF) for archiving the data and providing access, and the multiple funding agencies who support CMIP6 and ESGF. The data that were used in this study were provided by the HadGEM2-ES Development Team, the World Climate Research Programme's Working Group on Coupled Modelling, the Global Organization for Earth System Science Portals, the Earth System Grid Federation, the Centre for Environmental Data Analysis, and the Deutsches Klimarechenzentrum GmbH.

Supplementary Materials

In the supplementary material, the time series for the energy cycle components corresponding to the historical data (1929–2014) are presented. Figure s1 displays the time series for the energy forms, Figure s2 displays the time series for the energy conversions, and Figure s3 displays the time series for the energy generation and dissipation. (*Supplementary Materials*)

References

[1] G. I. Taylor, "Eddy motion in the atmosphere," *Philosophical Transactions of the Royal Society of London, Series A*, vol. 215, pp. 1–26, 1915.

[2] E. N. Lorenz, "Available potential energy and the maintenance of the general circulation," *Tellus*, vol. 7, no. 2, pp. 157–167, 1955.

[3] E. N. Lorenz, "Generation of available potential energy and the intensity of the general circulation," in *Dynamics of Climate*, R. L. Pfeffer, Ed., Pergamon Press, Oxford, UKpp. 86–92, 1960.

[4] E. N. Lorenz, *The Nature and Theory of the General Circulation of the Atmosphere*, World Meteorological Organization, Geneva, Switzerland, 1967.

[5] G. J. Boer and S. Lambert, "The energy cycle in atmospheric models," *Climate Dynamics*, vol. 30, no. 4, pp. 371–390, 2008.

[6] V. Eyring, S. Bony, G. A. Meehl et al., "Overview of the coupled model intercomparison project phase 6 (CMIP6) experimental design and organization," *Geoscientific Model Development*, vol. 9, no. 5, pp. 1937–1958, 2016.

[7] C. Pascoe, B. N. Lawrence, E. Guilyardi, M. Juckes, and K. E. Taylor, "Designing and documenting experiments in CMIP6," *Geoscientific Model Development Discussions*, 2019.

[8] K. Riahi, D. P. van Vuuren, E. Kriegler et al., "The Shared Socioeconomic Pathways and their energy, land use, and greenhouse gas emissions implications: an overview," *Global Environmental Change*, vol. 42, pp. 153–168, 2017.

[9] D. P. van Vuuren, E. Kriegler, B. C. O'Neill et al., "A new scenario framework for Climate Change Research: scenario matrix architecture," *Climatic Change*, vol. 122, no. 3, pp. 373–386, 2014.

[10] K. E. Taylor, R. J. Stouffer, and G. A. Meehl, "An overview of CMIP5 and the experiment design," *Bulletin of the American Meteorological Society*, vol. 93, no. 4, pp. 485–498, 2012.

[11] E. Kriegler, B. C. O'Neill, S. Hallegatte et al., "The need for and use of socio-economic scenarios for climate change analysis: a new approach based on shared socio-economic pathways," *Global Environmental Change*, vol. 22, no. 4, pp. 807–822, 2012.

[12] D. P. van Vuuren, S. J. Smith, and K. Riahi, "Downscaling socioeconomic and emissions scenarios for global environmental change research: a review," *Wiley Interdisciplinary Reviews: Climate Change*, vol. 1, no. 3, pp. 393–404, 2010.

[13] R. Dellink, J. Chateau, E. Lanzi, and B. Magné, "Long-term economic growth projections in the shared socioeconomic pathways," *Global Environmental Change*, vol. 42, pp. 200–214, 2017.

[14] B. C. O'Neill, E. Kriegler, K. L. Ebi et al., "The roads ahead: narratives for shared socioeconomic pathways describing world futures in the 21st century," *Global Environmental Change*, vol. 42, pp. 169–180, 2017.

[15] B. C. O'Neill, E. Kriegler, K. Riahi et al., "A new scenario framework for climate change research: the concept of shared socioeconomic pathways," *Climatic Change*, vol. 122, no. 3, pp. 387–400, 2014.

[16] M. J. Gidden, K. Riahi, S. J. Smith et al., "Global emissions pathways under different socioeconomic scenarios for use in CMIP6: a dataset of harmonized emissions trajectories through the end of the century," *Geoscientific Model Development*, vol. 12, no. 4, pp. 1443–1475, 2019.

[17] M. Margules, "Uber die Energie der Stürme (On the energy of storms- originally published by the Imperial Central Institute for Meteorology Vienna, Austria," in *The Mechanics of the Earth's Atmosphere- A Collection of Translations*, C. Abbe, Ed., Creative Media Partners, LLC, Sacramento, CA, USA,pp. 533–595, 1904.

[18] H. S. Muench, "On the dynamics of the wintertime stratosphere circulation," *Journal of the Atmospheric Sciences*, vol. 22, no. 4, pp. 349–360, 1965a.

[19] H. S. Muench, *Stratospheric Energy Processes and Associated Atmospheric Long-Wave Structure in Winter*, Office of Aerospace Research, Arlington, VI, USA, 1965b.

[20] S. C. Michaelides, "Limited area energetics of Genoa cyclogenesis," *Monthly Weather Review*, vol. 115, no. 1, pp. 13–26, 1987.

[21] E. C. Kung, "Large-scale balance of kinetic energy in the atmosphere," *Monthly Weather Review*, vol. 94, no. 11, pp. 627–640, 1966.

[22] J. A. Dutton and D. R. Johnson, "The theory of available potential energy and a variational approach to atmospheric energetics," *Advances in Geophysics*, vol. 12, no. C, pp. 333–436, 1967.

[23] A. H. Oort, "On estimates of the atmospheric energy cycle," *Monthly Weather Review*, vol. 92, no. 11, pp. 483–493, 1964.

[24] E. Oriol, "Energy budget calculations at ECMWF- Part 1: analyses 1980–81," ECMWF, Technical Report, 35, 1982.

[25] R. P. Pearce, "On the concept of available potential energy," *Quarterly Journal of the Royal Meteorological Society*, vol. 104, no. 441, pp. 737–755, 1978.

[26] E. N. Lorenz, "Energy and numerical weather prediction," *Tellus*, vol. 12, no. 4, pp. 364–373, 1960a.

[27] J. Van Mieghem, *Atmospheric Energetics*, Clarendon Press, Oxford, UK, 1973.

[28] A. F. Aranha and J. A. P. Veiga, "An analysis of the spectral energetics for a planet experiencing rapid greenhouse gas emissions," *Atmospheric and Climate Sciences*, vol. 07, no. 01, pp. 117–126, 2017.

[29] P. R. Bannon, "Atmospheric available energy," *Journal of the Atmospheric Sciences*, vol. 69, no. 12, pp. 3745–3762, 2012.

[30] M. J. Roberts, A. Baker, E. W. Blockley et al., "Description of the resolution hierarchy of the global coupled HadGEM3-GC3.1 model as used in CMIP6 HighResMIP experiments," *Geoscientific Model Development*, vol. 12, pp. 4999–5028, 2019.

[31] M. Roberts, *MOHC HadGEM3-GC-LL Model Output for CMIP6 HighResMIP Highres-Future, Version 20200326*, Earth System Grid Federation, 2018.

[32] P. Good, *MOHC HadGEM3-GC31-LL Model Output Prepared For CMIP6 ScenarioMIP ssp126, Version 20200419*, 2020.

[33] P. Good, *MOHC HadGEM3-GC31-LL Model Output Prepared For CMIP6 ScenarioMIP ssp245, Version 20200419*, 2020.

[34] P. Good, *MOHC HadGEM3-GC31-LL Model Output Prepared For CMIP6 ScenarioMIP ssp585, Version 20200419*, 2020.

[35] J. Ridley, M. Menary, T. Kuhlbrodt, M. Andrews, and T. Andrews, *MOHC HadGEM3-GC31-LL Model Output Prepared For CMIP6 Historical, Version 20200419*, 2019.

[36] M. B. Menary, T. Kuhlbrodt, J. Ridley et al., "Preindustrial control simulations with HadGEM3-GC3.1 for CMIP6," *Journal of Advances in Modeling Earth Systems*, vol. 10, no. 12, pp. 2018, MS001495–3075, 2018.

[37] T. Kuhlbrodt, C. G. Jones, A. Sellar et al., "The low-resolution version of HadGEM3 GC3.1: development and evaluation for global climate," *Journal of Advances in Modeling Earth Systems*, vol. 10, no. 11, pp. 2865–2888, 2018.

[38] K. D. Williams, D. Copsey, E. W. Blockley et al., "The Met Office global coupled model 3.0 and 3.1 (GC3.0 and GC3.1) configurations," *Journal of Advances in Modeling Earth Systems*, vol. 10, no. 2, pp. 357–380, 2018.

[39] S. Michaelides, "Lorenz atmospheric energy cycle in climatic projections," *Climate*, vol. 9, no. 12, p. 180, 2021.

[40] S. C. Michaelides, "A spatial and temporal energetics analysis of a baroclinic disturbance in the mediterranen," *Monthly Weather Review*, vol. 120, no. 7, pp. 1224–1243, 1992.

[41] E. Reiter, *Atmospheric Transport Processes- Part 1: Energy Transfers and Transformations*, R. TID-24868, Ed., U.S. Atomic Energy Commission, Washington, D.C, USA, 1969.
[42] D. Hernández-Deckers and J. S. von Storch, "Energetics responses to increases in greenhouse gas concentration," *Journal of Climate*, vol. 23, no. 14, pp. 3874–3887, 2010.
[43] Y. H. Kim and M. K. Kim, "Examination of the global lorenz energy cycle using MERRA and NCEP-reanalysis 2," *Climate Dynamics*, vol. 40, no. 5–6, pp. 1499–1513, 2013.
[44] Q. Ma, V. Lembo, and C. L. E. Franzke, "The Lorenz energy cycle: trends and the impact of modes of climate variability," *Tellus A: Dynamic Meteorology and Oceanography*, vol. 73, no. 1, Article ID 1900033, 2021.
[45] L. Li, A. P. Ingersoll, X. Jiang, D. Feldman, and Y. L. Yung, "Lorenz energy cycle of the global atmosphere based on reanalysis datasets," *Geophysical Research Letters*, vol. 34, no. 16, pp. 1–5, 2007.
[46] L. Boljka, T. G. Shepherd, and M. Blackburn, "On the coupling between barotropic and baroclinic modes of extratropical atmospheric variability," *Journal of the Atmospheric Sciences*, vol. 75, no. 6, pp. 1853–1871, 2018.
[47] V. Lembo, F. Lunkeit, and V. Lucarini, "TheDiaTo (v1.0) – a new diagnostic tool for water, energy and entropy budgets in climate models," *Geoscientific Model Development*, vol. 12, no. 8, pp. 3805–3834, 2019.
[48] U. Ulbrich and P. Speth, "The global energy cycle of stationary and transient atmospheric waves: results from ECMWF analyses," *Meteorology and Atmospheric Physics*, vol. 45, no. 3–4, pp. 125–138, 1991.
[49] M. D. Zelinka, T. A. Myers, D. T. McCoy et al., "Causes of higher climate sensitivity in CMIP6 models," *Geophysical Research Letters*, vol. 47, no. 1, 2020.
[50] Y. Dong, K. C. Armour, C. Proistosescu et al., "Biased estimates of equilibrium climate sensitivity and transient climate response derived from historical CMIP6 simulations," *Geophysical Research Letters*, vol. 48, no. 24, 2021.
[51] J. M. Gregory, W. J. Ingram, M. A. Palmer et al., "A new method for diagnosing radiative forcing and climate sensitivity," *Geophysical Research Letters*, vol. 31, no. 3, Article ID L03205, 2004.
[52] T. Andrews, M. B. Andrews, A. Bodas-Salcedo et al., "Forcings, feedbacks, and climate sensitivity in HadGEM3-GC3.1 and UKESM1," *Journal of Advances in Modeling Earth Systems*, vol. 11, no. 12, pp. 4377–4394, 2019.
[53] E. N. Lorenz, "Energetics of atmospheric circulation," in *International Dictionary of Geophysics*, Pergamon Press, Oxford, UK, 1965.
[54] J. M. Wallace and P. V. Hobbs, *Atmospheric Science- an Introductory Survey*, Elsevier, Amsterdam, The Netherlands, 2nd edition, 2006.
[55] P. Gleckler, "The AMIP experience: challenges and opportunities," in *Proceedings of the Second Phase of the Atmospheric Model Intercomparison Project (AMIP2), toward Innovative Model Diagnostics, WCRP/WGNE Workshop*, P. J. Gleckler, Ed., pp. 11–14, Toulouse, France, November, 2005.
[56] G. J. Boer, "Some dynamical consequences of greenhouse gas warming," *Atmosphere-Ocean*, vol. 33, no. 4, pp. 731–751, 1995.
[57] V. Lucarini, K. Fraedrich, and F. Lunkeit, "Thermodynamics of climate change: generalized sensitivities," *Atmospheric Chemistry and Physics*, vol. 10, no. 20, pp. 9729–9737, 2010.
[58] J. A. P. Veiga and T. Ambrizzi, "A global and hemispherical analysis of the Lorenz energetics based on the representative concentration pathways used in CMIP5," *Advances in Meteorology*, vol. 2013, pp. 1–13, 2013.
[59] P. Marquet, "On the concept of exergy and available enthalpy: application to atmospheric energetics," *Quarterly Journal of the Royal Meteorological Society*, vol. 117, no. 499, pp. 449–475, 1991.
[60] R. Knutti, R. Furrer, C. Tebaldi, J. Cermak, and G. A. Meehl, "Challenges in combining projections from multiple climate models," *Journal of Climate*, vol. 23, no. 10, pp. 2739–2758, 2010.
[61] Y. Díaz-Esteban, G. B. Raga, and O. O. Díaz Rodríguez, "A weather-pattern-based evaluation of the performance of CMIP5 models over Mexico," *Climate*, vol. 8, no. 1, p. 5, 2020.
[62] S. Kravtsov, "Pronounced differences between observed and CMIP5-simulated multidecadal climate variability in the twentieth century," *Geophysical Research Letters*, vol. 44, no. 11, pp. 5749–5757, 2017.
[63] C. Miao, Q. Duan, Q. Sun et al., "Assessment of CMIP5 climate models and projected temperature changes over Northern Eurasia," *Environmental Research Letters*, vol. 9, no. 5, p. 055007, 2014.